



# Emplacement of shocked basement clasts during crater excavation in the Ries impact structure

Fabian Dellefant<sup>1</sup> · Lina Seybold<sup>1,2</sup> · Claudia A. Trepmann<sup>1</sup> · Stuart A. Gilder<sup>1</sup> · Iuliia V. Sleptsova<sup>1</sup> · Stefan Hölzl<sup>1,2</sup> · Melanie Kaliwoda<sup>1,3</sup>

Received: 15 August 2023 / Accepted: 8 March 2024  
© The Author(s) 2024

## Abstract

In the Aumühle quarry of the Ries impact structure, moderately shocked clasts from the Variscan basement occur sandwiched between overlying suevite and components derived from the Mesozoic sedimentary cover of the underlying Bunte Breccia without distinct shock effects. We analyzed the clasts by optical microscopy, scanning electron microscopy (SEM/EDS/EBSD), and Raman spectroscopy to unravel their emplacement relation to the overlying suevite and the sediment-rock clasts of the Bunte Breccia. Clasts sizes range up to few decimeters and are embedded in a fine-grained lithic matrix; no impact-melt fragments are observed. Amphibolite clasts contain maskelynite with few lamellar remnants of feldspar, indicating shock pressures of 28–34 GPa. Amphiboles have cleavage fractures and  $(\bar{1}01)$  mechanical twins suggesting differential stresses > 400 MPa. Felsic gneiss components have optically isotropic SiO<sub>2</sub> indicative of shock pressures ≈ 35 GPa. Metagranite cataclasite clasts contain shocked calcite aggregates and quartz with a high density of fine rhombohedral planar deformation features indicating shock pressures ≈ 20 GPa. The moderately shocked basement clasts originate from deeper levels of the transient cavity and lower radial distance to the center of the structure compared to the sediment-rock clasts. Both were ballistically ejected during crater excavation. In accordance with palaeo- and rock magnetic data, they were mixed during turbulent deposition at the top of the Bunte Breccia before the emplacement of suevite. The high amount of basement clasts below suevite and on top of the underlying Bunte Breccia is consistent with the commonly reported inverse stratigraphy in the Ries impact structure.

**Keywords** Relative impactite emplacement · Inverse stratigraphy · Crater excavation stage · Shock effects

## Introduction

The Nördlinger Ries is one of the best-preserved terrestrial impact structures, where the impact rocks of the two dominating ejecta, the impact-melt-bearing suevites and the impact-melt-free *Bunte Trümmersmassen* (German for

multi-coloured debris masses), are well-exposed and studied intensely since the 1960s. Yet, the emplacement and relationship of the various impact breccias are still a matter of debate (e.g., Kring 2005; Wünnemann et al. 2005; Tartèse et al. 2022; Sleptsova et al. 2024). Polymict impact breccias consist of components from different positions within the impact structure, reflecting significant variations in shock conditions and diverse lithologies from various pre-impact stratigraphic positions. These breccias carry crucial information about the relative displacements occurring from excavation to deposition.

In this study, we present the shock effects from moderately shocked (10–50 GPa) Variscan basement clasts mixed together with apparently unshocked (i.e., no observed shock effects except for fractures and being part of an impact breccia) sediment-rock clasts with the *Bunte Trümmersmassen* at the bottom and suevite at the top in the Aumühle quarry in the Nördlinger Ries (Fig. 1). Relatively few occurrences

✉ Fabian Dellefant  
fabian.dellefant@lmu.de

<sup>1</sup> Department of Earth and Environmental Sciences, Ludwig-Maximilians-Universität München, Theresienstr. 41, 80333 Munich, Germany

<sup>2</sup> RiesKraterMuseum Nördlingen (RKM), Bavarian Natural History Collections, Eugene-Shoemaker-Pl. 1, 86720 Nördlingen, Germany

<sup>3</sup> Mineralogical State Collection Munich (MSM), Bavarian Natural History Collections, Theresienstr. 41, 80333 Munich, Germany

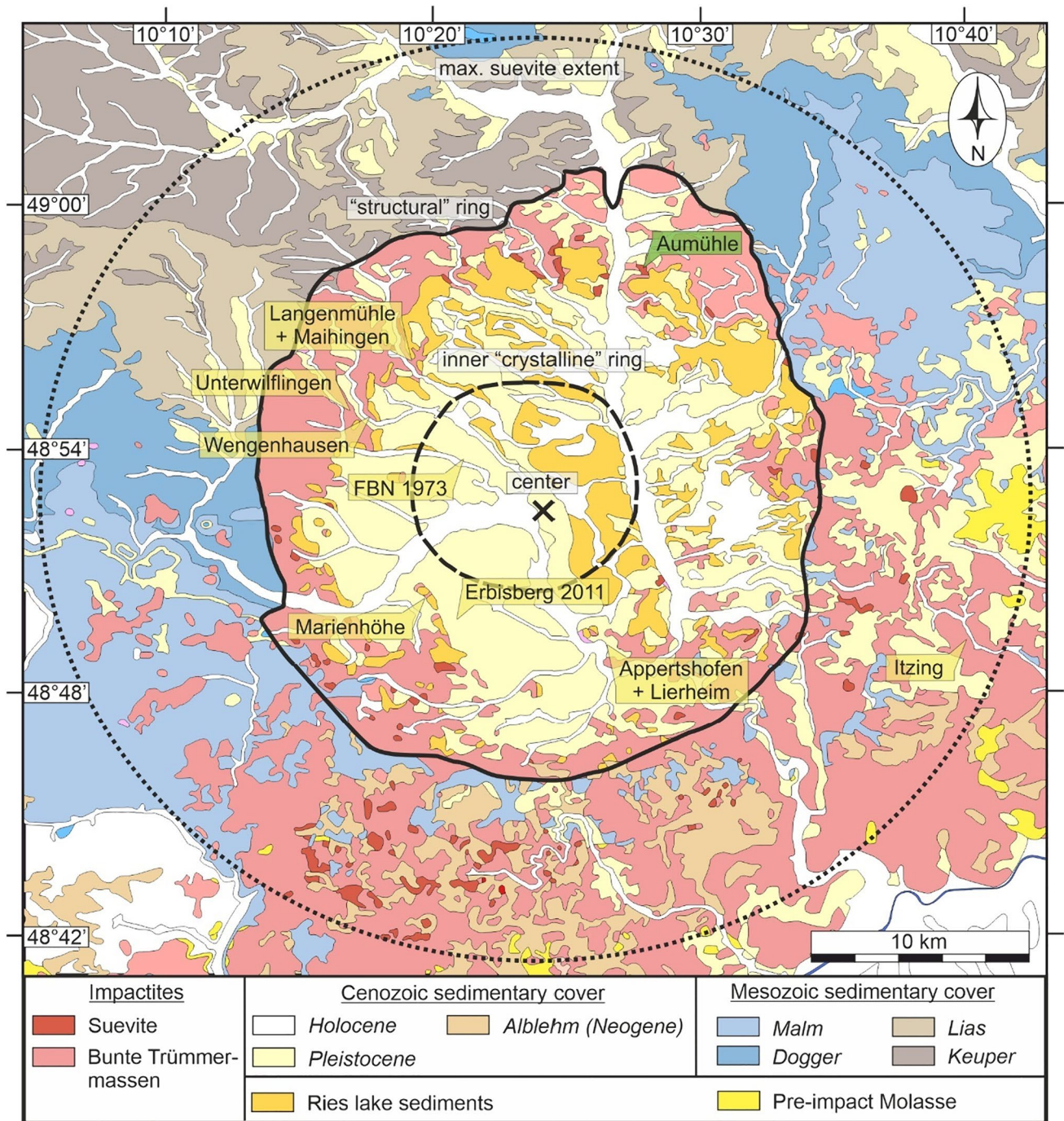


**Fig. 1** Simplified geological map of the Ries impact structure with occurrences of moderately shocked basement clasts associated to the *Bunte Trümmersmassen* [yellow (Abadian 1972; Graup 1978; Stöfler 1977; Chao et al. 1987; Arp et al. 2019; Seybold et al. 2022,

2023; Tartèse et al. 2022) and green for this study]. Map edited after: The General Geological Map of the Federal Republic of Germany 1:250,000 (GÜK250), © Bundesanstalt für Geowissenschaften und Rohstoffe (BGR)

of moderately shocked, impact-melt-free basement dominated impact breccias are documented in the Nördlinger Ries (Fig. 1); their contact to the sediment-rock-dominated components of the *Bunte Trümmersmassen* and to the suevite is rarely exposed. A direct contact of shocked crystalline

basement clasts to sediment-rock components of the *Bunte Trümmersmassen* and to the overlying suevite at the Ries was recently documented by Sleptsova et al. (2024) and offers the unique occasion to investigate their relation and emplacement. Here, we characterize the shock effects of the

basement clasts and describe the field occurrence of both the overlying suevite and the underlying sediment-rock components of the Bunte Breccia. Based on our field observations and findings on the shock conditions, we discuss in combination with the complementary magnetic characterization of the rocks by Sleptsova et al. (2024) the relative displacements from excavation to deposition.

### The Ries impact structure and its impact breccias

The 22–26 km diameter Ries impact structure was formed by a meteorite impact  $\approx 14.7$  Ma ago (Di Vincenzo 2022; Lange and Suhr 2022 and references therein). The target rocks comprise the approximately 700 m thick Mesozoic sedimentary sequence of the Swabian-Franconian Alb and the underlying Variscan basement, mainly composed of amphibolites, metagranites, and paragneisses (e.g., Graup 1978; von Engelhardt and Graup 1984; Hüttner and Schmidt-Kaler 1999; Tartèse et al. 2022). Stöffler et al. (2013) distinguish five major structural features of the impact structure: I) the central basin  $r < 6$  km, II) the uplifted inner crystalline ring  $r \approx 6$  km, III) the megablock zone  $r \approx 6$ –13 km, IV) the structural rim  $r \approx 13$ –14 km, and V) the outer continuous ejecta blanket  $r \approx 13$ –45 km. Two dominating ejecta blankets are distinguished in the Ries, the ballistically ejected lithic, impact-melt-free *Bunte Trümmersmassen* and the impact-melt-bearing suevite (e.g., Stöffler et al. 2013 and references therein, Sturm et al. 2015).

The *Bunte Trümmersmassen* consists of allochthonous rotated rocks that originate from the sedimentary cover and the Variscan basement, which were fragmented and displaced during the formation of the crater (Pohl et al. 1977; Hüttner and Schmidt-Kaler 1999; Stöffler et al. 2013; Sturm et al. 2015). It forms the volumetrically dominant impact breccia deposit in the Ries (Hörz et al. 1983; Sturm et al. 2015). The *Bunte Trümmersmassen* comprises (i) the *Bunte Breccia* with components  $< 25$  m and (ii) the megablocks of  $> 25$  m in size. Both typically show relatively low shock conditions and are dominated by sediment-rock components (e.g., Abadian 1972; Pohl et al. 1977; Hörz et al. 1983; von Engelhardt and Graup 1984; von Engelhardt 1990; Hüttner and Schmidt-Kaler 1999; Stöffler et al. 2013; Sturm et al. 2015). Variscan basement megablocks cover less than 10% of the area covered by all megablocks (Sturm et al. 2015). These basement megablocks commonly display few shock effects, such as kink bands in biotite, implying weak shock conditions (5–10 GPa; von Engelhardt and Graup 1984; von Engelhardt 1990; Stöffler et al. 2013). The clasts in the Bunte Breccia are likewise dominantly derived from the sedimentary cover rocks that experienced relatively low shock conditions ( $P < 10$  GPa,  $T < 100$  °C; e.g., Hörz et al. 1983; von Engelhardt 1990; Stöffler and Grieve 2007). About 3–10% of the lithic clasts of the Bunte Breccia are

derived from the Variscan basement that experienced higher yet various shock conditions ( $< 10$ –50 GPa; e.g., Stöffler 1971a; Abadian 1972; Pohl et al. 1977; Graup 1978; Stöffler and Ostertag 1983; von Engelhardt 1990). Those parts of the Bunte Breccia that comprise moderately shocked (10–50 GPa) basement rocks of various lithologies have been distinguished as “polymict crystalline breccia” (Stöffler 1971a; Abadian 1972; Graup 1978; Von Engelhardt 1990). Abadian (1972) distinguished three types of polymict crystalline breccias: I) isolated complexes with no relationship to their surroundings (Leopold-Meyers-Keller); II) occurrences with components likely derived from the adjacent basement megablocks (Appetshofen + Lierheim, Itzing); and III) breccia dikes with material different to the basement megablocks in which they occur (Maihingen-Klostermühle/Langenmühle) (Abadian et al. 1973; von Engelhardt 1990; Arp et al. 2019). The basement megablocks at Langenmühle comprise various foliated Variscan gneisses and metagranites. Cataclastically deformed calcite-bearing metagranites can contain shock-twinned calcite (Seybold et al. 2023). Quartz in the metagranites can contain planar deformation features (PDFs) indicative of 10 to 15 GPa shock pressures (Tartèse et al. 2022). The nearby basement blocks at Unterwilflingen show weak shock conditions (5–10 GPa, Stöffler et al. 2013; Seybold et al. 2022; Tartèse et al. 2022). Furthermore, cataclastic dikes consisting of mixed basement and few sediment-rock clasts occur within the basement at depths of up to 1187 m, as found in the FBN1973 research drill core north of Nördlingen (Stöffler et al. 1977). These dikes are interpreted as a result of a highly energetic emplacement during the early excavation stage of the cratering process (Stöffler 1977). No shock pressure estimations were reported for the veins (Graup 1977; Hüttner 1977; Stöffler 1977; Stöffler et al. 1977– see Schmidt-Kaler (1977) for more information on the crystalline basement lithologies in the research drill core FBN1973). At the inner ring, polymict crystalline breccia was found from 55.5 to 62.43 m in the Erbisberg drill core 2011 located above upper Triassic sandstone blocks from the Bunte Breccia and below intact gneiss blocks and monomict crystalline breccias (Arp et al. 2019). The components of the *Bunte Trümmersmassen* commonly occur in the Ries impact structure with an inverse stratigraphy, i.e., stratigraphically lower pre-impact units can be overlain by upper units (e.g., Pohl 1977; Sturm et al. 2015). Consistently, the polymict crystalline breccia typically occurs at the top layer of the Bunte Trümmersmassen (Abadian 1972).

Suevites are per definition of Stöffler and Grieve (2007): “polymict impact breccia with particulate matrix containing lithic and mineral clasts in all stages of shock metamorphism including cogenetic impact melt particles, which are in a glassy or crystallised state” (Pohl et al. 1977; Stöffler et al. 2013, 2018). At Ries, the minerals and lithic clasts of the matrix and the impact melt particles, the so-called *Flädle*,

are derived mainly from the Variscan basement (e.g., Pohl et al. 1977; Stöffler and Grieve 2007; Reimold et al. 2013, Stöffler et al. 2013 and references therein, Osinski et al. 2016). Shock effects in suevites indicate a broad range of shock conditions (e.g., felsic components from low shock conditions up to F-S6; von Engelhardt et al. 1995; Stöffler and Grieve 2007; Stöffler et al. 2018; Stähle et al. 2022). Suevite occurs inside the inner ring on top of the crystalline basement (crater suevite), outside the inner ring on top of *Bunte Trümmersmassen* (outer suevite), and as dikes within the parautochthonous crater basement as well as within displaced crystalline megablocks, i.e., dike suevites (e.g., Stöffler 1977; Stöffler et al. 2013 and references therein).

## Samples

We investigate the microstructures and shock effects of basement clasts at the top of the *Bunte Trümmersmassen* directly overlain by suevite at the Aumühle quarry of the Ries impact structure (Figs. 2, 3; Sleptsova et al. 2024). The Aumühle suevite quarry is located in the north-northeastern part about 11 km from the impact structure center in the megablock zone (N 48°58'16.00" E 10°37'47.60, Fig. 1–3), between the inner crystalline ring and the structural rim. There, the magnetic properties of rocks sampled in a profile from the Bunte Breccia to the suevite were investigated by Sleptsova et al. (2024). The suevite is characterized by a thermal remanent magnetization carried by magnetite with directions parallel to the palaeomagnetic field at the time of the impact (reverse to the present-day field; e.g., Pohl et al. 1977). About 10 cm from the contact with the Bunte Breccia, hematite concentrations increase due to hydrothermal alteration. In contrast, the remanent magnetization directions of the clasts at the top of the Bunte Breccia fall into two groups: the first group has moderately shocked basement clasts with chemical remanent magnetization (CRM) carried by titanohematite with directions that vary widely among each clast. The titanohematite is interpreted to have acquired its CRM during impact cratering and the clasts were rotated during turbulent deposition. In contrast, the second group within the sediment-rock clasts show CRM carried by magnetite with directions parallel to the reversed field (parallel to that of the suevite). It is interpreted that the magnetite grew during hydrothermal alteration after turbulent deposition. Based on these findings, Sleptsova et al. (2024) proposed a three-stage model of (1) turbulent deposition of the impact melt-free breccia with clast rotation at temperatures < 580 °C, (2) deposition of the overlying suevite, which acted as a semi-permeable barrier that confined hot (< 300 °C) oxidizing fluids to the permeable breccia zone, and (3) prolonged hydrothermal activity producing further alteration with growth of magnetite in the sediment-rock clasts which ended before the next geomagnetic reversal.

These findings indicate that (1) the basement clasts as well as the sediment-rock clasts at the top of the Bunte Breccia were deposited before the suevite and (2) a different shock and emplacement history during impact cratering of the basement clasts and the sediment-rock components of the Bunte Breccia compared to the overlying suevite, which is investigated in this study.

## Methods

Fieldwork was conducted between 2020 and 2023 with the main sampling on the 15th of September 2020. Due to the ongoing excavation in the quarry, the investigated part of the outcrop (Fig. 2a) as also described by Kroepelin et al. (2022), is now partly removed or covered. Polished and uncovered thin sections (25 µm) were prepared from 30 samples and investigated by polarization microscopy (Leica DM2700 P). For analytical microscopy, one amphibolite clast (sample R20-4,5; Fig. 2a, b), one gneiss clast (sample R20-14; Fig. 2a, c), one metagranite cataclasite clast (sample R20-2; Fig. 2a, d), and one sandstone clast (sample R20-8; Fig. 2a, e) were selected. Photomicrographs were taken with a Leica MC170 HD camera and processed with the Leica Application Suite X 3.08.19082 software.

Raman spectroscopy was conducted for phase determination with a HORIBA JOBIN YVON XploRa ONE micro-Raman system at the Mineralogical State Collection Munich (SNSB). The system is equipped with a Peltier-cooled CCD detector and edge filters. An 1800 g/mm grating and a 532 nm (green) 2ω-Nd:YAG laser were used. Slit and hole diameters were 100 and 300 µm, respectively, combined with an integration time of 5 × 5 s. For maskelynite, feldspar, and amphibole, 50% laser power was applied, whereas diaplectic SiO<sub>2</sub> glass was measured with 25% laser power corresponding to max. 5.4 mW or max. 2.5 mW, respectively. A 100× long working distance objective resulted in a 0.9 µm laser spot size on the sample surface. Wavelength calibration was performed with a pure Si-wafer chip on the predominant 520 cm<sup>-1</sup> peak. The precision in the Raman peak position is estimated at ± 1.5 cm<sup>-1</sup>.

Samples were studied with a Hitachi SU5000 scanning electron microscope (SEM) equipped with a backscattered electron (BSE) detector, energy-dispersive X-ray spectroscopy (EDS) detector (Oxford Instruments), NordlysNano high-sensitivity electron backscatter diffraction (EBSD) detector (Oxford Instruments), and field emission gun. SEM observations used accelerating voltages of 10–20 kV and a working distance of 10–25 mm. Thin sections were chemo-mechanically polished with a colloidal alumina suspension (Syton with particle size of 0.04 µm) for EBSD analysis to reduce the surface damage from preparation. A sample holder tilted at 70° with respect to the electron beam was

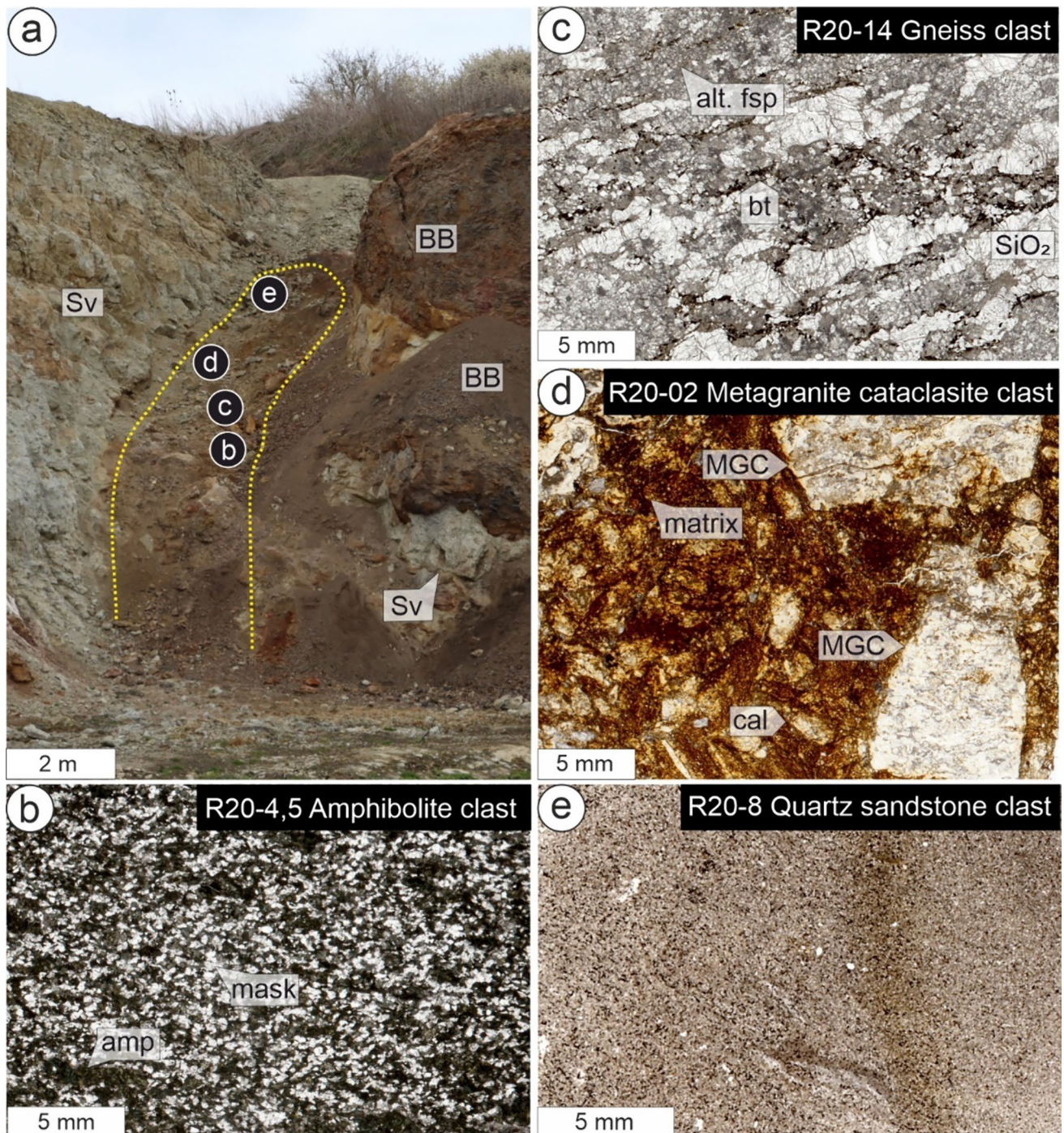


**Fig. 2** Locations of samples R20-4,5 (**b**), R20-14 (**c**), R20-2 (**d**), and R20-8 (**e**) in the Aumühle quarry at the top of the Bunte Breccia (BB) (Fig. 3). The occurrence of the basement clasts is indicated by the yellow dashed line. Note that suevite (Sv) locally occurs as lens within Bunte Breccia. Thin section scans from **b** amphibolite clast

R20-4,5 (amp: amphibole, mask: maskelynite; Figs. 4, 5), **c** gneiss clast R20-14 (alt. fsp.: altered feldspar, bt: biotite; Fig. 6), **d** Metagranite cataclasite clast R20-2 (MGC: metagranite clast, cal: calcite; Figs. 7, 8), and **e** quartz sandstone clast R20-8 (Fig. 9)

used. EDS and EBSD data were acquired and processed with AZtec software (versions 4.2 and 6.0). For EBSD data acquisition, we used the *Inorganic Crystal Structure Database* (Bergerhoff et al. 1983). Step sizes for automatic EBSD

mapping were chosen between 0.5  $\mu\text{m}$  and 1  $\mu\text{m}$  depending on the EBSD-pattern quality and the size of the microstructure of interest. EBSD data were interpreted by the Channel 5 and the AZtecCrystal softwares (Oxford Instruments).

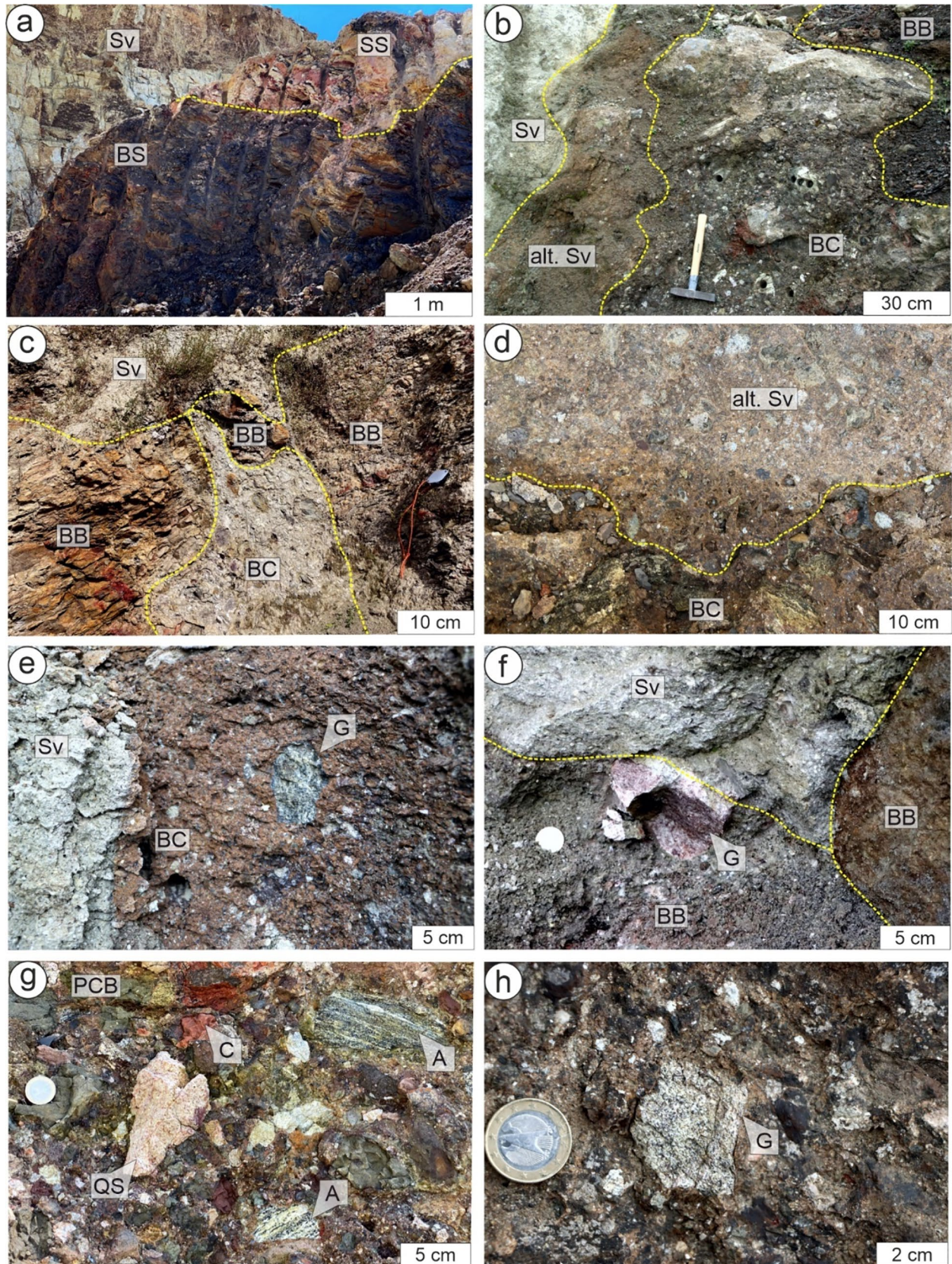


**Fig. 3** Occurrence of basement clasts at the top of the Bunte Breccia and at the bottom of the suevite at Aumühle quarry, location of photographs (b–h) is indicated by yellow dashed line in Fig. 2a. **a** Sediment-rock components of the Bunte Breccia with inverse stratigraphy are lower Jurassic black shales (BS) overlain by upper Triassic sandstones (SS). Note the suevite (Sv) in the background. **b** Sharp contacts of suevite (Sv), altered suevite (alt. Sv), basement-clast rich horizon (BC), and sediment-rock component of Bunte Breccia (BB). **c** Vein-like occurrence of basement-clast rich horizon (BC) between sediment-rock components of Bunte Breccia (BB, iron sandstone middle Jurassic) covered by suevite (Sv). **d–f** Sharp contact of altered suevite (alt. Sv), grey suevite (Sv), and Bunte Breccia (BB) to basement-clast rich horizon (BC) with granitoid clasts (G). **g, h** Basement clasts mixed with sediment-rock clasts in fine-grained lithic matrix [A=amphibolite in **g**, G=gneiss in **h**] and sediment-rock clasts [C=clay stone; QS=quartz sandstone in **g**]

Single pixels different from the surrounding pixels and non-indexed points were replaced with the orientation extrapolated from seven surrounding pixels. All stereograms are equal-angle projections of the lower hemisphere given with the number of datapoints (n).

## Results

### Field occurrence of basement clasts

The contact between the impact-melt-free Bunte Breccia at the bottom and the overlying impact-melt-fragment-bearing suevite in the Ries impact structure is well-exposed at the Aumühle quarry (Fig. 2a; e.g., von Engelhardt 1997; Hüttner and Schmidt-Kaler 1999; Osinski et al. 2004; Stöffler et al. 2013). The contact is irregular, where suevite can occur as veins or lenses within the components of the Bunte Breccia (Fig. 2a). At the northeastern corner of the Aumühle quarry, the clasts in the Bunte Breccia range from a few cm up to 15 m in diameter (Figs. 2a, 3a–c). Upper Jurassic black shales are overlain by upper Triassic sandstones (Fig. 3a), consistent with an inverse stratigraphy (e.g., Pohl 1977; Sturm et al. 2015).

Clasts of felsic gneisses and amphibolites mixed with sandstones and clay stones occur embedded in a fine-grained lithic matrix with diameters of few cm to dm (generally < 1 m) at the base of the suevite and at the top of larger sediment-rock components of the Bunte Breccia, commonly with diameters > 1 m (Figs. 2, 3b–d). Mesoscopically, no evidence of impact melt fragments were found. The overlying matrix-rich and matrix-supported suevite with mm to dm-sized well-preserved impact melt fragments and fine-grained to few cm-sized lithic components are typically relatively fresh and grey (Figs. 2a, 3a, b, e, f). At the contact to the Bunte Breccia, however, the suevite can locally be altered (Fig. 3b, d), where it is red colored due to fine-dispersed hematite (Sleptsova et al. 2024).

The contact between the basement-clast-rich horizon to both (altered) suevite and the sediment-rock components of the Bunte Breccia is sharp, without a gradual transition of clast sizes and lithologies (Fig. 3b–f).

## Shock effects

### Maskelynite and mechanical ( $\bar{1}01$ ) amphibole twins in amphibolite clast

The amphibolite (sample R20-4,5; Fig. 2a, b) has a weak foliation defined by aligned elongate grains with long axes of 300  $\mu\text{m}$  to few mm of amphibole and an optically isotropic transparent phase (Fig. 4a–d). The latter has a stoichiometric feldspar composition (typically andesine with  $\text{Na}_{0.5-0.6}\text{Ca}_{0.4-0.5}\text{Al}_{1.4-1.5}\text{Si}_{2.5-2.6}$  per formula unit) as indicated by EDS measurements. In contrast to the amphibole, the optically isotropic phase with feldspar composition shows generally no electron backscattered diffraction patterns (EBSP) indicated by very low band contrast (black in Fig. 4e). This phase is interpreted as maskelynite (diaplectic feldspar) with typical broad Raman peaks of approximately 457, 510, and 586  $\text{cm}^{-1}$  (Fritz et al. 2005) depicting main Raman peaks at 482 and 509  $\text{cm}^{-1}$  (Fig. 4f), indicative of feldspar (Mernagh 1991). Locally, in the core of maskelynite “grains”, lamellae with grey birefringence can optically be identified (Fig. 4c, d), which are indexed by EBSD as feldspar (yellow lamellae in Fig. 4e). Therefore, these lamellae are interpreted as remnants of the former feldspar.

The optical birefringence and pleochroism of amphibole (Fig. 4a, b) as well as EDS measurements with Mg/(Mg+Fe) ratio of 0.6–0.7 and 6.5–7.6 Si per formula indicate actinolite and magnesio-hornblende compositions (Leake et al. 1997). Comparing the Raman spectra of the shocked amphibole and an actinolite standard show main peaks at approximately 667  $\text{cm}^{-1}$ , with full width at half maximum values of 40  $\text{cm}^{-1}$  and 15  $\text{cm}^{-1}$ , respectively (Fig. 4f). This broadening in the respective peaks is interpreted to result from deformation during shock.

Shock effects in the amphibole are cleavage fractures along  $\{110\}$  and twins parallel to  $(\bar{1}01)$  (Figs. 4a, d, 5). The twins are characterized by a  $(\bar{1}01)$  twin plane, a misorientation axis parallel  $[101]$ , and a misorientation angle of  $\approx 180^\circ$  (Fig. 5a, b). Such  $(\bar{1}01)[101]$  twins are known from high-stress crystal plasticity associated with pseudotachylite formation (Brückner and Trepman 2021). The cleavage fractures parallel  $\{110\}$  are typically deflected by the  $\{101\}$  twin boundaries (Fig. 5c, d). The twin lamellae can be wedge-shaped and bent (Fig. 5a) and are typically fine-lamellar with widths mostly smaller than 5  $\mu\text{m}$  (Fig. 5c–d), as characteristic for mechanical twins. The twin density can be up to 0.3/ $\mu\text{m}$  (Fig. 5c–d).

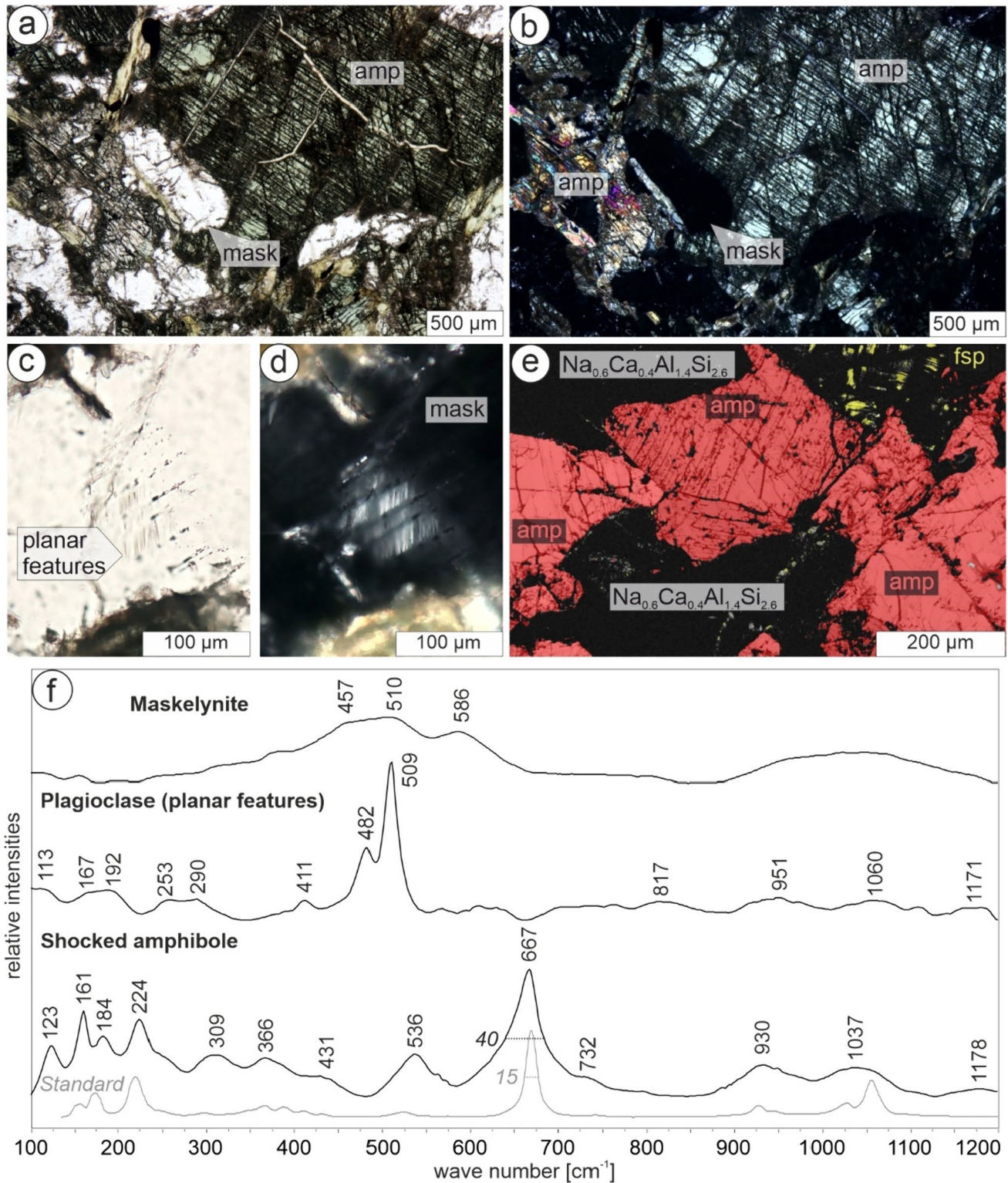


**Fig. 4** Amphibolite clast (sample R20-4.5; Fig. 2a, b). **a, b** Polarized light micrographs of amphibole (amp) with planar features and optically isotropic maskelynite (mask), **b** is taken with crossed polarizers. **c, d** Polarized light micrographs of maskelynite (mask) with lamellae of residual feldspar (planar features); **c** taken with crossed polarizers. **e** EBSD map showing the band contrast and colored by indexed phase: amphibole (amp; red) and feldspar lamellae (fsp; yellow).

Maskelynite with the same feldspar composition is indicated by dark band contrast (no EBSD). **f** Raman spectra of maskelynite, feldspar (lamellae), shocked amphibole, and an amphibole standard [grey; RRUFF actinolite standard (R050025)]. Note that the full width at half maximum of shocked amphibole and the actinolite standard are given in italics



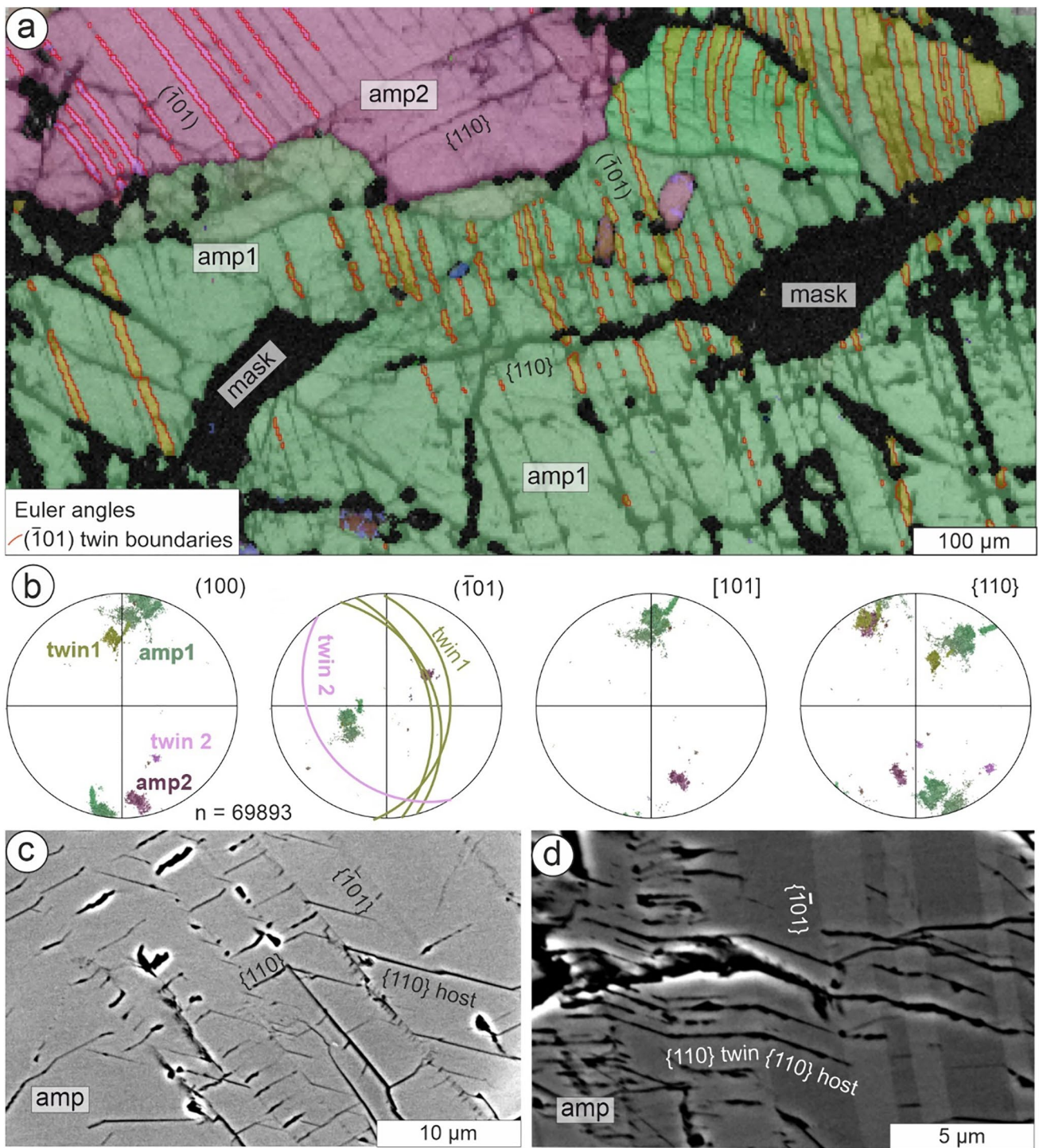


**Fig. 5** Twinned amphibole within an amphibolite clast (sample R20-4,5; Fig. 2a, b). **a**, **b** EBSD orientation map (Euler angle coloring) of amphibole grains (amp1 and amp2) with twin boundaries (red) and respective stereographic projections (lower hemisphere) of (100), ( $\bar{1}01$ ),

[101] and {110} poles/directions with ( $\bar{1}01$ ) great circles for the twin boundaries. **c**, **d** BSE image of amphibole (amp) with ( $\bar{1}01$ ) twins and {110} cleavage fractures

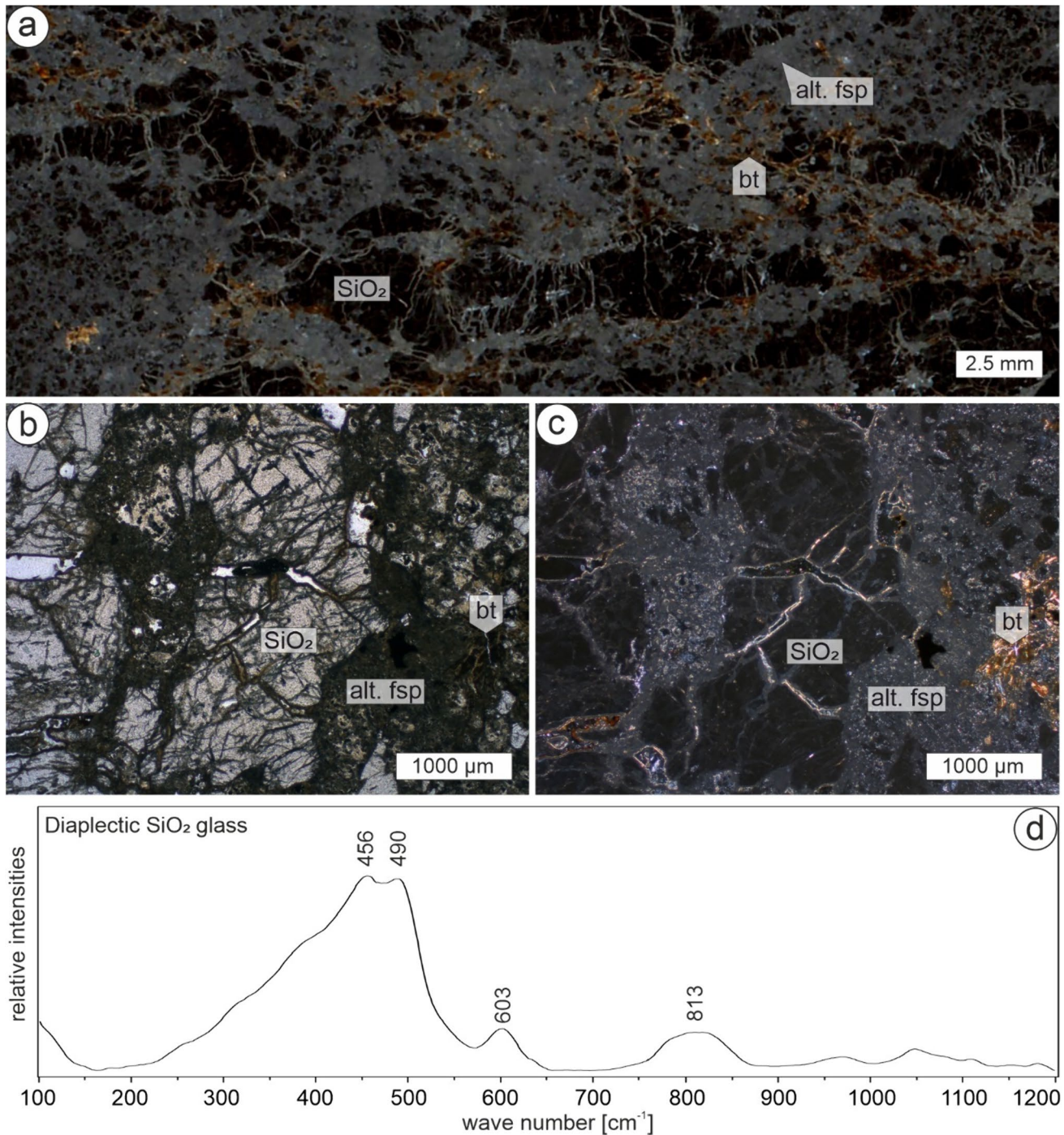


**Fig. 6** Gneiss clast (sample R20-14; Fig. 2a, c). **a–c** Diaplectic  $\text{SiO}_2$  glass ( $\text{SiO}_2$ ), altered feldspar (alt. fsp), and biotite (bt) within foliation fabric of the gneiss host in polarized light; **a, c** are taken with crossed polarizers. **d** Raman spectrum of diaplectic  $\text{SiO}_2$  glass

### Diaplectic $\text{SiO}_2$ glass in gneiss clast

The gneiss clast has a foliation characterized by elongate grains with long axes of several mm of altered feldspar and optically isotropic  $\text{SiO}_2$  (sample R20-14; Fig. 2a, c),

interpreted as former quartz (Fig. 6a–c). Biotite is often associated with the altered feldspar (Fig. 6a, c). The optically isotropic diaplectic  $\text{SiO}_2$  glass is characterized by main broad Raman peaks (Fig. 6d) approximately at 456, 490, 603, and 813  $\text{cm}^{-1}$  (Kowitz et al. 2013).

## Metagranite cataclasite clast

The metagranite cataclasite (sample R20-2; Fig. 2a, d) consists of a Fe-rich, fine-grained, lithic matrix rich in phyllosilicates, which encloses 100  $\mu\text{m}$  to 1 cm angular and foliated metagranite clasts composed of shocked feldspar and quartz (Fig. 7a, b). Quartz has a mottled undulatory extinction and a high density of PDFs (Fig. 7c–g). Although the shocked quartz is birefringent (Fig. 7c), it has a very poor band contrast of the EBSD, where indexing was only rarely possible (Fig. 7d). In these cases, an orientation of the most dominant PDFs parallel to  $\{10\bar{1}3\}$ ,  $\{01\bar{1}3\}$  and  $\{01\bar{1}2\}$  is indicated (Fig. 7d–g).

Calcite aggregates occur embedded within the cataclasite matrix, with the long axis of the aggregates ranging up to 1 mm (Figs. 7a, 8a). The calcite aggregates are fractured with fragment sizes from 10 s of  $\mu\text{m}$  to 100 s of  $\mu\text{m}$  (Fig. 8a–d). The calcite aggregate comprises deformed grains with twins and an internal misorientation and undeformed grains devoid of any internal deformation microstructures (Fig. 8b–d, g). The deformed grains (relative dark band contrast in Fig. 8b) show misorientation angles deviating from the grain average orientation of up to  $23^\circ$  (yellow–red colors in Fig. 8d), whereas the undeformed grains (bright band contrast in Fig. 8b) deviate in orientation by less than  $5^\circ$  (blue color Fig. 8d). The deformed grains contain *e*-twins characterized by a twin plane parallel to  $\{01\bar{1}8\}$  (turquoise lines in Fig. 8c, e) and *r*-twins characterized by twin boundaries parallel to  $\{10\bar{1}4\}$  (blue lines in Fig. 8c, e). Twins in deformed grains that show a high number of pores are truncated by undeformed grains (white arrows in Fig. 8d, f), indicating that the undeformed grains grew and replaced deformed crystal volumes.

## Sediment-rock clast

The sandstone (sample R20-8; Fig. 2a, d) has grain diameters between 5 to 40  $\mu\text{m}$ , comprising quartz, phyllosilicates, and  $\approx 5\%$  limonite as well as some hematite grains (Fig. 9). No apparent shock effects except for fractures, i.e., no shock effects that indicate shock pressures, were observed, consistent with the study of Sleptsova et al. (2024).

## Discussion

### Shock and deformation conditions

The shock effects observed in the basement clasts are summarized in Table 1. For the amphibolite clast, diaplectic glass with andesine composition (Fig. 4) indicates shock pressures range from 20 to 34 GPa (Schaal and Hörz 1977; Ostertag 1983; Stöffler et al. 2018), equivalent to shock

stages M-S3 to M-S4 (Stöffler et al. 2018) or shock stages IIa to IIb according to the IUGS system (Stöffler and Grieve 2007). The  $(\bar{1}01)[101]$  mechanical twins in amphibole (Fig. 5) indicate crystal plastic deformation at high differential stresses. The  $(\bar{1}01)[101]$  twinning in amphibole has been documented in pseudotachylytes (e.g., Brückner and Trepmann 2021), other meteorite craters (Chao 1967), as well as in nuclear explosion sites (Borg 2013). According to the experimentally calibrated critical resolved shear stress of 200–400 MPa (Rooney et al. 1970), differential stresses of  $\geq 400$  MPa are required for  $(\bar{1}01)[101]$  twinning of amphibole (Brückner and Trepmann 2021). Stähle et al. (2022) documented shock veins within shocked amphibolite clasts (shock stages M-S3 to M-S4) in suevite from the Ries impact structure, which is not apparent in the amphibolite clast of our study.

Diaplectic  $\text{SiO}_2$  glass in the gneiss clast (Fig. 6) indicates shock pressures of 35–50 GPa (Stöffler 1971b, 1972; Stöffler and Hornemann 1972; Kowitz et al. 2013), which can therefore be classified as shock stage F-S5 (Stöffler et al. 2018) or shock stage II according to the IUGS system (Stöffler and Grieve 2007). Biotite without adjacent thermal decomposition products, such as fine-grained hematite or magnetite, indicates temperatures below 600  $^\circ\text{C}$  (Wones and Eugster 1965).

The metagranite cataclasite clast (R20-2, Figs. 7, 8) contains quartz grains with a high density of fine rhombohedral PDFs (Fig. 7c–g). Shock pressures thus range from 10 to 20 GPa (Hörz 1968; Müller and Hornemann 1969; Stöffler and Langenhorst 1994; Holm-Alwmark et al. 2018), representing shock stages F-S2 to F-S3 (Stöffler et al. 2018) or shock stage Ia according to the IUGS system (Stöffler and Grieve 2007). The cataclasite clast with metagranite and calcite components compares lithologically well to metagranite cataclasites from the Langenmühle outcrop at Maihingen and samples from the FBN1973 research drill core described by Seybold et al. (2023), however, the recorded shock conditions were found to be relatively low ( $< 7$  GPa), as no PDFs in quartz were observed. There, the calcite is interpreted to originate from pre-impact hydrothermal veins within metagranites from the Variscan basement. Differential stresses of few GPa were inferred by the high density of fine-lamellar calcite twins ( $> 1/\mu\text{m}$ ) with simultaneous activation of all known twin systems in one grain (*e*-, *r*-, and *f*-twins as well as so-called *a*-type domains). Also in the cataclasite described here (Fig. 8), the fine-lamellar calcite twins are interpreted to represent shock effects given the simultaneous activation of *e*- and *r*-twins in one grain (Fig. 8c, e, f), the narrow widths of few  $\mu\text{m}$ , and the straight twin boundaries with no evidence of twin boundary migration (Fig. 8g). New grains that overgrew the shocked and deformed calcite grains (Fig. 8b–d, f) indicate higher strain during shock and/or higher temperatures after shock compared to the samples

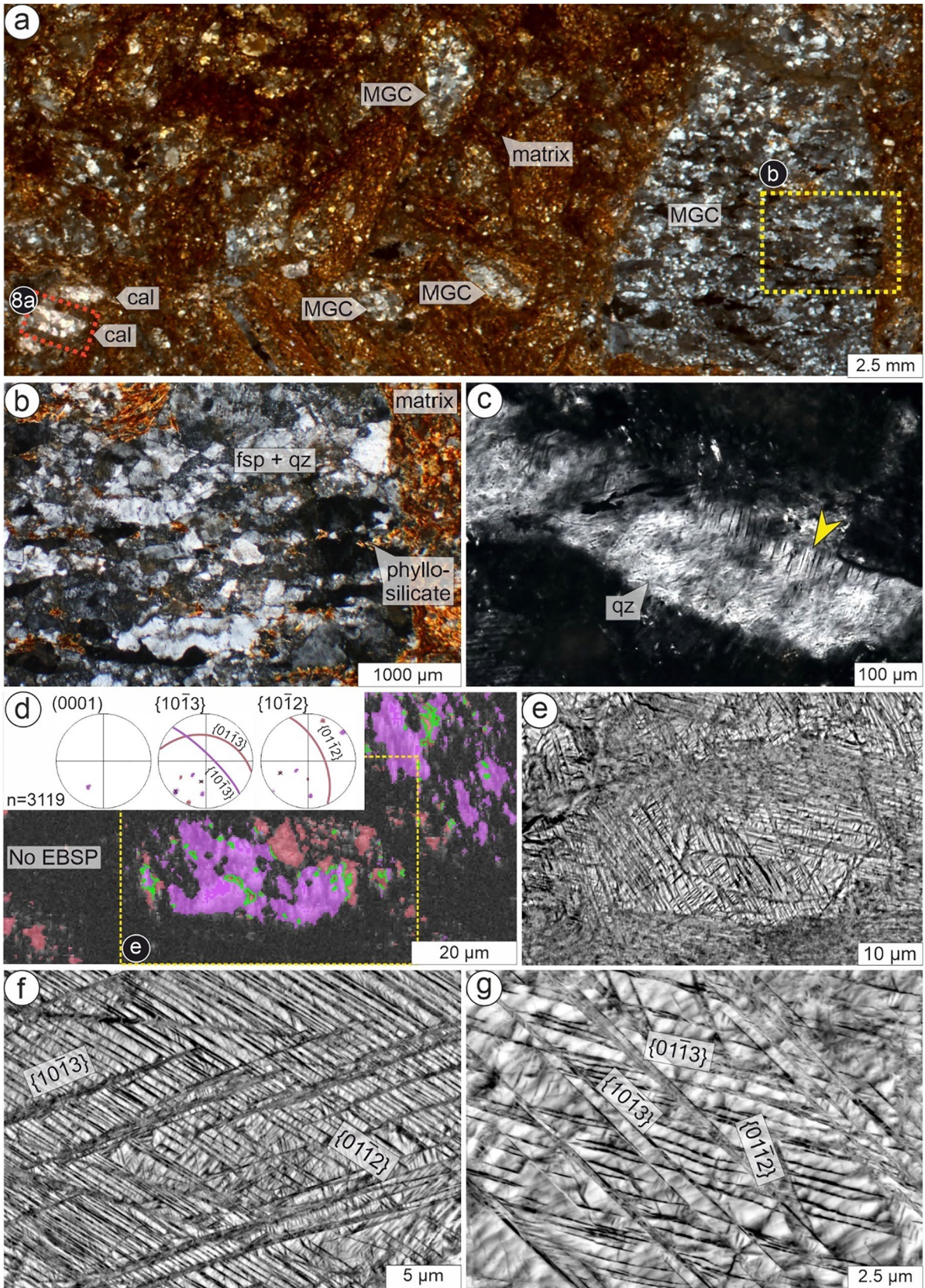


**Fig. 7** Metagranite cataclasite clast (sample R20-2; Fig. 2a, d). **a** Overview with metagranite clasts (MGC) and fragmented calcite (cal) clasts in a fine-grained Fe-rich matrix; thin section scan with crossed polarizers. The yellow rectangle indicates the area magnified in **b** and the red rectangle depicts the area magnified in Fig. 8a. **b** Foliated metagranite clast composed of feldspar and quartz (fsp+qz) with adjacent phyllosilicate-rich matrix; polarized light micrograph, crossed polarizers. **c** Quartz (qz) within metagranite cataclasite clast with PDFs (yellow arrow); polarized light micrograph, crossed polarizers. **d** EBSD orientation map (Euler angle coloring) with pole figures of quartz with PDFs parallel to  $\{10\bar{1}3\}$  and  $\{01\bar{1}2\}$ . Note that the black areas yield no EBSD; Dauphiné twin boundaries are shown by green lines. Yellow dashed line indicates BSE image shown in **e**. **e** BSE image of part of the mapped area shown in **d**. **f, g** BSE images with close up of quartz with PDFs

described by Seybold et al. (2023), consistent with the evidence of PDFs in quartz grains (Fig. 7c–g). The occurrence of cataclasites within the breccia (Figs. 2d, 7a, 8a) requires two stages of fracturing. An initial stage of “in situ” fracturing of the calcite-vein bearing metagranites forming calcite cemented cataclasites and subsequent fracturing and incorporation as clast into the breccia.

In the sediment-rock clasts (sample R20-8; Fig. 9), no distinct shock effects, no planar fractures or other planar features, no high-pressure polymorphs, and/or glass (Kieffer et al. 1976; Kowitz et al. 2016) were detected. Therefore, the shock stages SR-S1 (Stöffler et al. 2018) or 0 according to the IUGS system (Stöffler and Grieve 2007) are indicated.

### Relation of the shocked basement clasts to polymict crystalline breccia and the *Bunte Trümmersmassen*

The shock conditions of the basement clasts of different rock types with shock pressures ranging from 10 to 50 GPa and differential stresses of  $\geq 400$  MPa (Figs. 4, 5, 6, 7, 8), compare well with observation from those of polymict crystalline breccias associated to the Bunte Trümmersmassen in the Ries (e.g., Abadian 1972; Graup 1978; von Engelhardt 1990; Tartése et al. 2022). Therefore, the basement-clast-rich horizon described here may be correlated with such polymict crystalline breccias. However, we observe a significantly higher number of apparently unshocked sediment-rock clasts (Fig. 9), and there is no association with only weakly shocked crystalline megablocks, as common for most occurrences of polymict impact breccias (e.g., Unterwilflingen, Maihingen/Klostermühle/ Langenmühle). Furthermore, the moderately shocked basement clasts observed here directly overlie the sediment-rock-dominated Bunte Breccia and are themselves directly overlain by suevite (Figs. 2, 3).

The type locality of the polymict crystalline breccia from the Nördlinger Ries is Meyers Keller, where it occurs as an irregular body on top of the Bunte Breccia (e.g., Abadian 1972; Abadian et al. 1973; Graup 1978). In contrast at the Aumühle quarry, the layer enriched in basement clasts is

overlain by suevite (Fig. 3a, b, f), whereas in Meyers Keller, Ries lake sediments overlie the breccia. Similarly, in the Erbisberg drill core (Arp et al. 2019), polymict crystalline breccia was detected on top of Bunte Breccia, which contains, like in Meyers Keller and Aumühle, highly shocked material (up to 35 GPa, Arp et al. 2019) and no impact melt products. Yet, in the Erbisberg drill core, polymict crystalline breccia is overlain by intact gneiss blocks and monomict crystalline breccia of the *Bunte Trümmersmassen* (Arp et al. 2019). The apparent systematic structural position on top of the Bunte Breccia at Meyers Keller (Abadian 1972), Aumühle (this study), and Erbisberg drill core (Arp et al. 2019) indicates the deposition of the polymict crystalline breccia *after* the deposition of the *Bunte Trümmersmassen*.

The emplacement of the *Bunte Trümmersmassen* is interpreted as a ballistic sedimentation, which results in a ground-level debris flow (Oberbeck 1975; Hörz et al. 1983) or/and an emplacement by a rolling-gliding base surge (Chao et al. 1987). The first model is an analogue to ejecta formations on the Moon under dry conditions without an atmosphere (Oberbeck 1975). A continuous *Bunte Trümmersmassen* deposit with a reduced thickness at  $\approx 1.00$ – $1.45$  Rc (crater radii) compared to a thicker accumulation at  $\approx 1.45$ – $2.12$  Rc resembling a moat and rampart morphology was revealed by Sturm et al. (2013) through an analysis of the Ries *Bunte Trümmersmassen* thickness. The model of a rolling-gliding base surge (Chao et al. 1987) is based on observations, such as striations on rock surfaces (e.g., Chao 1976; Chao et al. 1987), plastic deformation of carbonate rock and clay ironstone at isostatic pressures of  $\approx 3$  GPa, plastic flow and tight folding of clay-bearing rocks of distant units (Chao et al. 1987), as well as the occurrence of thick Bunte Breccia deposits in pre-Ries valleys and lowlands (Bader and Schmidt-Kaler 1977). Ductile deformation during emplacement is reported by Pietrek and Kenkmann (2016) based on observations of folding, twisting, and smearing of Tertiary clays, which also occur wrapped around component clasts. Furthermore, the latter authors explain granular flow and the generation of deformation patterns as a result of vaporization of pore water in sand- and siltstones.

### Relation of the basement clasts to the overlying suevite

In contrast to all other known outcrops of polymict crystalline breccia, the moderately shocked basement clasts in the Aumühle quarry are overlain directly by suevite (Figs. 2a, 3b–f). The sharp boundary to the suevite (Fig. 3b–f), the missing evidence of impact melt fragments, and the occurrence of larger basement and sediment-rock components (Fig. 3f, g) compared to the suevite clearly separates the basement-clast-rich horizon from the latter. Furthermore, the basement clasts systematically do not show a reversed

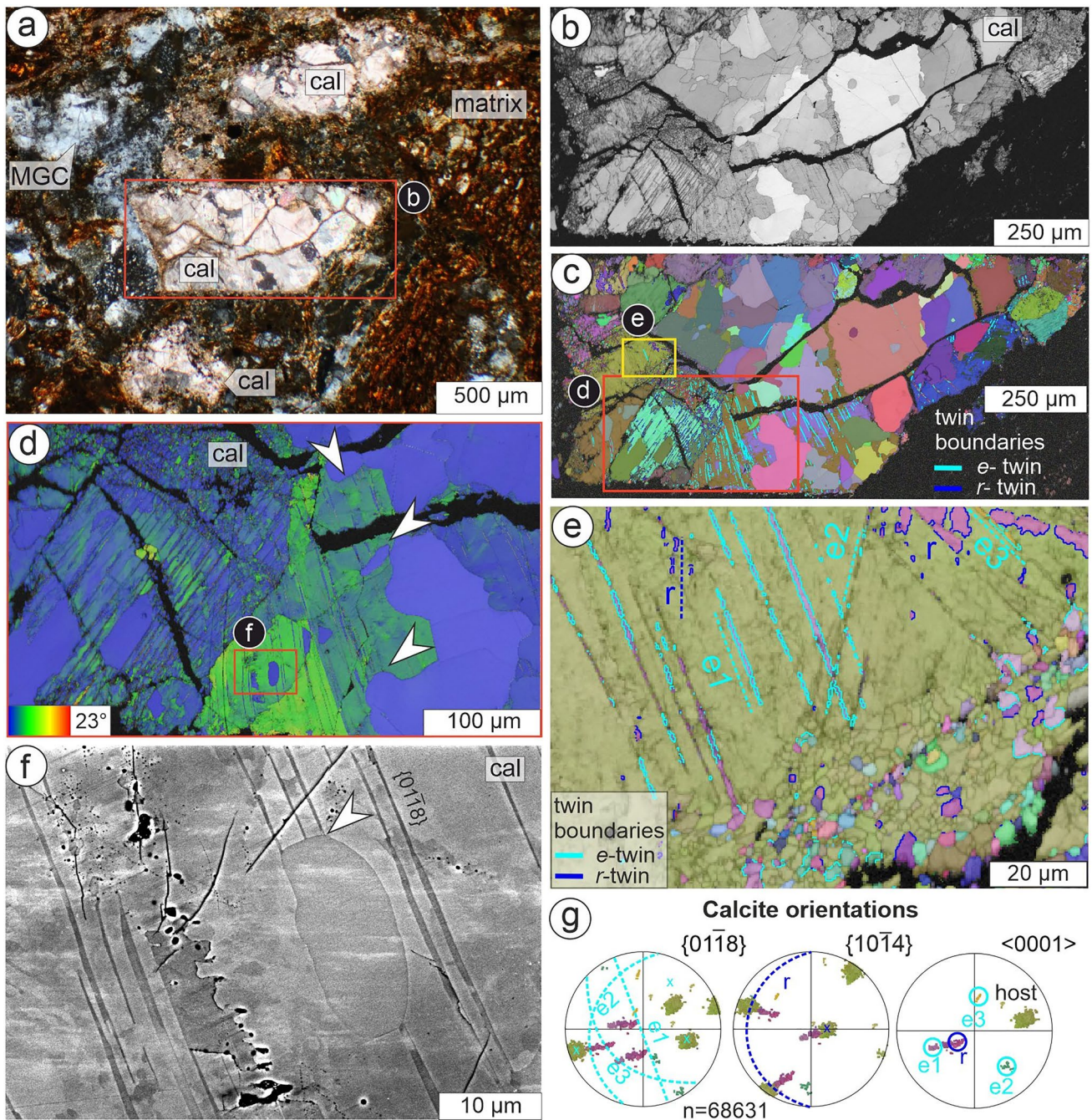


**Fig. 8** Shock effects of fractured calcite (cal) aggregate within cataclasite (sample R20-2; Fig. 2a, d). **a** Polarized light micrograph (crossed polarizers) of calcite aggregates (cal) and metagranite clasts (MGC) in fine-grained, phyllosilicate-rich matrix. Red line shows the position of EBSD data presented in **b–g**. **b** Band contrast map and **c** orientation map (Euler angle coloring) of the area displayed by the red line in **a**. The red and yellow rectangles in **c** indicate the position of EBSD maps shown in **d** and **e**, respectively. **d** Grain Reference Orientation Distribution map (GROD) displaying the angular deviation from the average grain orientation. Position of the shown

area is indicated by the red line in **c**. The arrows point to new grains overgrowing twinned grains. The red rectangle marks the position of the BSE image shown in **f**. **e** Orientation map (Euler angle coloring) of a twinned grain, which is partly replaced by a new grain (white arrow). Note the pores (black) within the twinned calcite. **g** Pole figures of calcite planes in **e** parallel to  $\{01\bar{1}8\}$ , and  $\{10\bar{1}4\}$  planes as well as  $\langle 0001 \rangle$  axes. The *r*-twin boundaries are displayed by blue and *e*-twin boundaries by turquoise lines and great circles

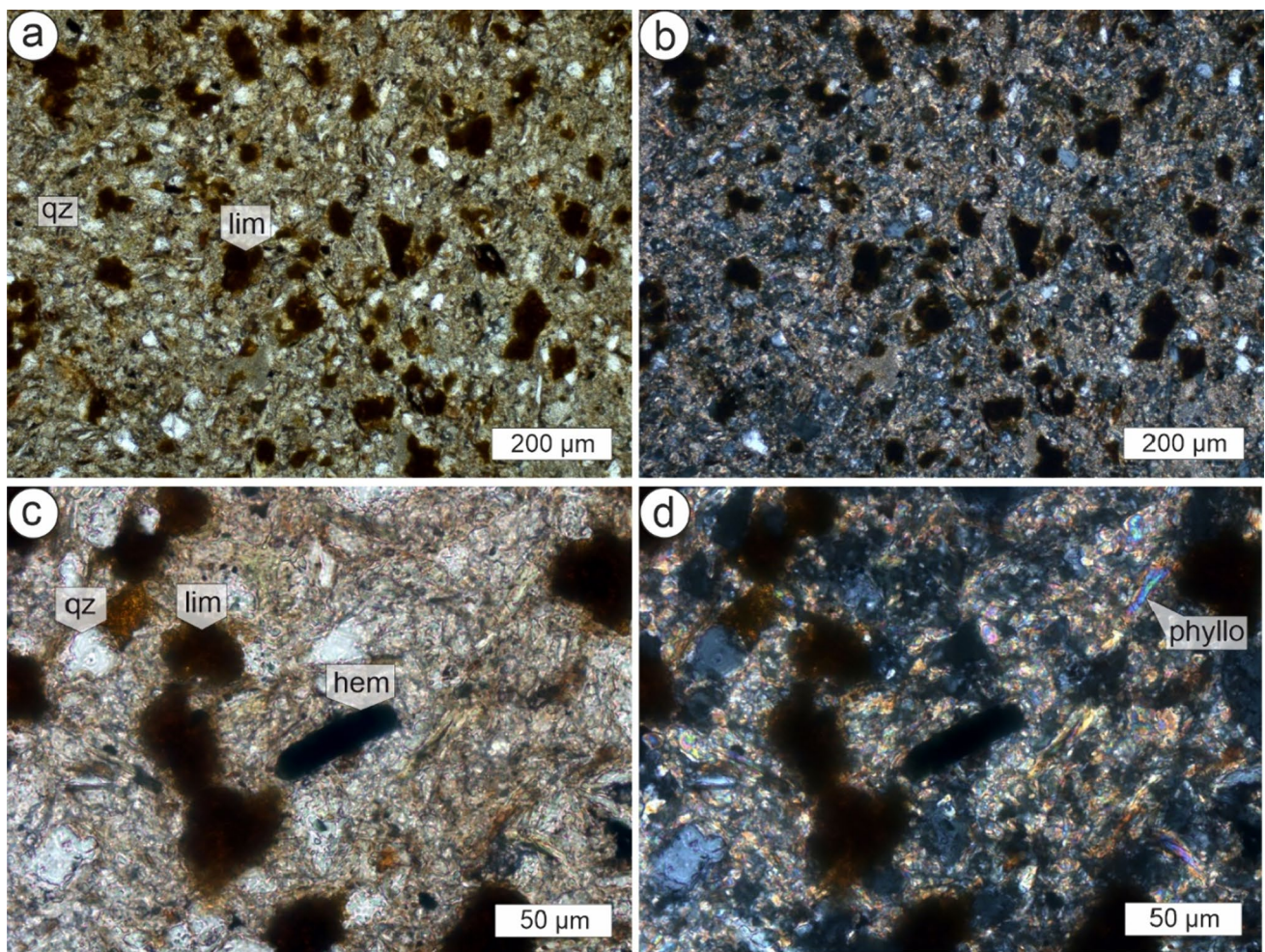


**Fig. 9** Polarized light micrographs of quartz sandstone clast (sample R20-8; Fig. 2a, e). Quartz (qz) and limonite (lim) grains occur together with local hematite (hem) grains within a matrix of phyllo-

silicates (phyllo). No apparent shock effects were observed; **a** and **b** as well as **c** and **d** are pairs of the same region with the same magnification, respectively; **b** and **d** are taken with crossed polarizers

**Table 1** Summary of shock stage classifications after Stöfler et al. (2018) of the different lithologies investigated in the shocked basement clasts of this study with the respective shock pressure interpretations. (Qz = quartz; Amp = amphibole; Fsp = feldspar; PDFs = planar deformation features)

Sample	Clast Lithology	Shock effects	Shock conditions	Shock Stage
R20-4,5	Amphibolite; Figs. 2a, b, 4, 5	Amp twins; diaplectic Fsp with lamellae	P = 20–34 GPa	M-S3 to M-S4
R20-14	Gneiss; Figs. 2a, c, 6	diaplectic SiO <sub>2</sub>	P = 34–50 GPa	F-S5
R20-2	Metagranite cataclasite; Figs. 2a, d, 7, 8	fracturing; PDFs in Qz, calcite twins	P = 1–20 GPa	F-S2 to F-S3
R20-8	Sandstone; Figs. 2a, e, 9	None	P < 1 GPa	SR-S1

magnetic polarity (Sleptsova et al. 2024) as the suevites elsewhere in the Nördlinger Ries (e.g., Pohl et al. 1977; Koch et al. 2012). Except at the very base, the suevite has magnetite as magnetic carrier and possesses tightly grouped palaeomagnetic directions corresponding to the Ries direction (chron C5ADR) at the time of the impact as a result of the deposition temperature above the Curie temperature of

magnetite (580 °C) creating a thermal remanent magnetization. The basement clasts described in our study were found by Sleptsova et al. (2024) to possess stable remanent magnetizations with randomly oriented palaeomagnetic directions for clasts with hematite as magnetic carrier, whereas clasts dominated by magnetite have the Ries direction. Based on the application of a partial thermal remanent magnetization

in the laboratory, Sleptsova et al. (2024) determined that the magnetization of the hematite-bearing clasts was blocked before rotation and that the temperature of the post-Ries hydrothermal system was below 300 °C.

Emplacement of the outer suevite is proposed as the collapse of an ejecta plume (von Engelhardt 1997), deposition of an impact melt flow (Osinski 2004), via lateral flow (Bringemeier 1994; Meyer et al. 2011), density flow (Newsom et al. 1990), or through a collapse of a post-impact phreatomagmatic plume system, which evolved from a fuel–coolant interaction of an aquifer or water with an impact melt sheet (Artemieva et al. 2013; Stöffler et al. 2013). Siegert et al. (2017) proposed an emplacement by a radial, granular fluid-based particulate density current similar to ignimbrite formation of volcanic systems. In neither of these emplacement scenarios, an accumulation of basement clasts is expected at the base of the suevite. If the basement-rich clast horizon resulted from mixing and reworking of the Bunte Breccia and suevite during turbulent emplacement, then we would expect to observe the presence of impact melt fragments and smaller basement clasts, like in the overlying suevite. The high amount of basement clasts at the top layer of the Bunte Breccia at Aumühle is mixed with apparently unshocked sediment-rock components. Furthermore, sharp layer contacts (Figs. 2a, 3b–e) and a notable absence of impact-melt fragments in the basement-clast-enriched layer indicate that the suevite was deposited independently and after the emplacement of the basement clasts on top of the Bunte Breccia, which is in accordance with the different magnetic properties (Sleptsova et al. 2024).

### Emplacement of the basement clasts

Dike occurrences of lithic breccias are reported from the Ries (FBN1973 research drill core, Stöffler 1977) and various other impact structures: the Rochechouart impact structure (e.g., Lambert 1981; Bischoff and Oskierski 1987), the Slate island impact structure (e.g., Dressler and Sharpton 1997), the Lockne impact structure (e.g., Sturkell and Ormö 1997), and the Chesapeake Bay impact structure (e.g., Wright Horton et al. 2009). These observations indicate that polymict lithic breccias often occur as dikes within the crystalline basement and basement megablocks, in contrast to the isolated complexes of irregular bodies, as observed in the Aumühle quarry (Figs. 2, 3). The dike breccias are generally characterized as matrix- or clast-supported injection veins of a few cm to several m in width and > 1 km in length (i.e., polymict clastic-matrix breccias in Dressler and Reimold 2004; polymictic clastic matrix breccias in Dressler and Sharpton 1997). Similar to the basement clasts described here, they comprise mostly shocked fragments from all stratigraphic levels of the pre-impact target (e.g., Abadian 1972; Abadian et al. 1973; Stöffler 1977; Lambert 1981;

Bischoff and Oskierski 1987). The emplacement of polymict crystalline breccia as dikes is interpreted as a highly energetic process, which takes place during the growth of the crater when shocked and fragmented material moves against and along the transient crater wall and intrudes it with a high particle motion (e.g., Stöffler 1977; Lambert 1981). The injected material is transported from 10 s of m to a few km (e.g., Stöffler 1977; Dressler and Sharpton 1997). The necessary energies as a function of pressure for the emplacement were only sufficient during the shock compression and the excavation stage of crater formation (Bischoff and Oskierski 1987). The mathematical *Maxwell Z-model* (Maxwell 1977; Croft 1980) was originally developed to predict the geometry of late-stage incompressible flow. In the context of impact cratering, the Z-model is employed to establish the geometric characteristics of the lift-out flow. Material is either ballistically ejected outwards along flow-fields except for a central cone-shaped volume, where material from within the impact center is interpreted to move horizontally or vertically along the transient crater wall (Bischoff and Oskierski 1987). The amount of the ballistically ejected material depends on the geometry of the excavation cavity, which has the same diameter as the transient cavity with about one third of its depth (Croft 1980). The amount of ballistically ejected material is hard to estimate given the highly energetic and turbulent excavation stage, however, the emplaced basement clasts have the same composition as the injected material (Fig. 10).

The occurrence of moderately shocked basement clasts at the top and between apparently unshocked sediment-rock clasts of the Bunte Breccia and directly at the base of the suevites at Aumühle quarry (Figs. 2a, 3b–e) suggests their emplacement as predicted by the *Maxwell Z-model* (Maxwell 1977; Croft 1980). After the incipient crater formation, where temperatures vaporized the target rock (Fig. 10a), melting and fracturing occur with increasing distance to the impact crater, respectively, upon unloading from shock compression (Davies 1972; Melosh 1989). The cataclasis (Figs. 2d, 7a, 8a) likely formed during this initial stage after passage of the shock wave by in-situ cataclasis of Variscan metagranite with pre-existing calcite veins (Fig. 10a), whereas brecciation with fragmentation of the basement clasts and transport of the clasts occurred upon subsequent crater excavation (Fig. 10b). The shocked and fragmented clasts from the Variscan basement were either ballistically ejected by cratering flow-fields consistent with an inverse stratigraphy (Maxwell 1977; Croft 1980) or injected into fractures within the transient excavation cavity wall (Bischoff and Oskierski 1987; Fig. 10b). At Aumühle, the basement clasts were subsequently deposited on the Bunte Breccia layer, which formed by a ground level debris flow (Oberbeck 1975; Hörz et al. 1983) and /or a rolling-gliding base surge (Chao et al. 1987; Fig. 10c). Further ballistically



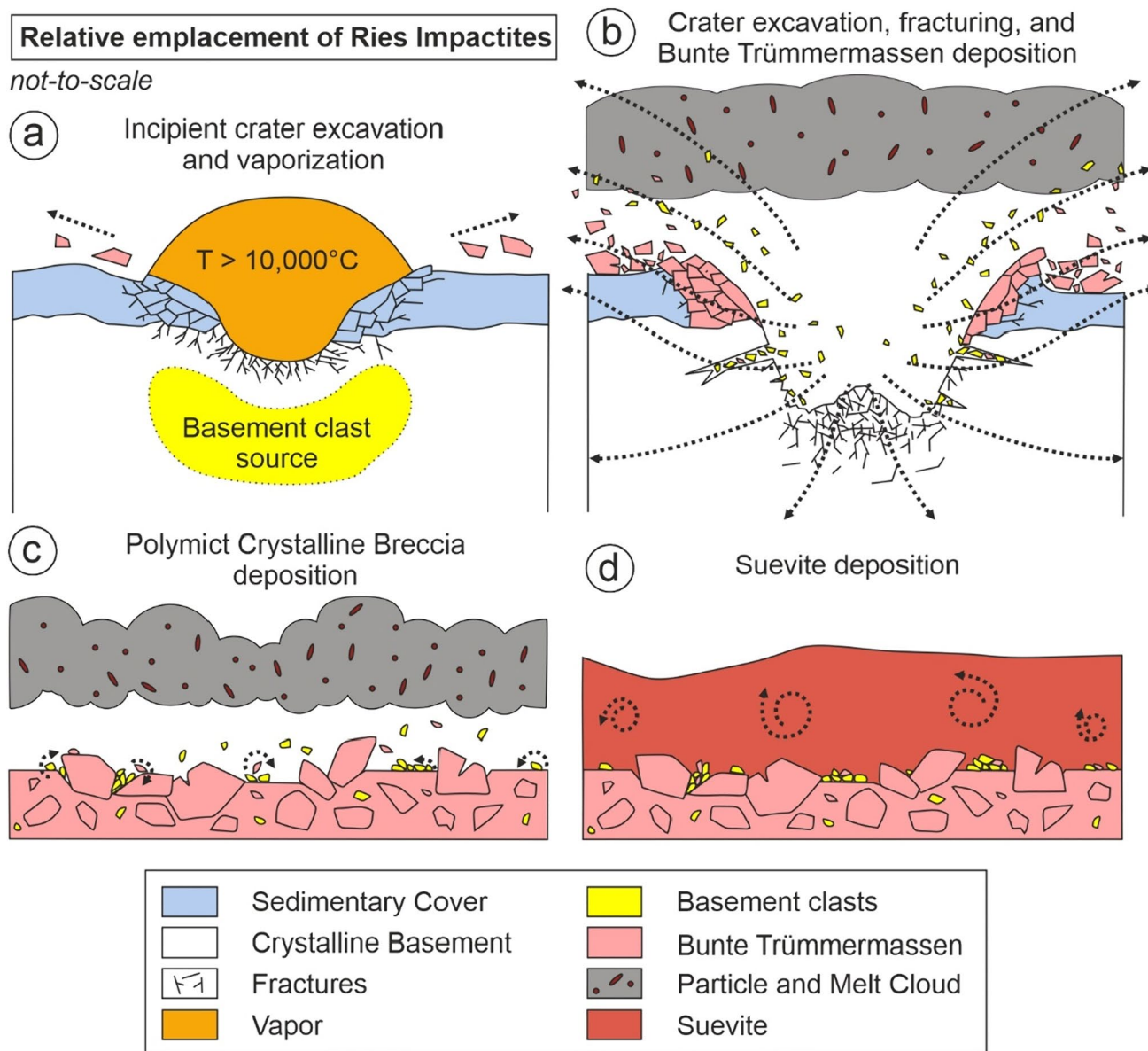


**Fig. 10** Relative emplacement of Ries impactites (not-to-scale). **a** Upon incipient crater excavation, *Bunte Trümmermassen* are ejected from the crater periphery. In the center of the crater cavity, temperatures lead to rock vaporization (Davies 1972; Melosh 1989). The yellow area indicates the source of the shocked basement clasts. **b** Ongoing crater excavation results in the formation of a fine-grained particle and melt cloud. Crater excavation leads to enhanced fracture generation within the crystalline basement and the overlying sedi-

mentary cover sequence. Shocked basement clasts move along flow-fields (black dashed lines) and are partially injected into the newly formed fracture system. However, fragmented clasts are also ejected outwards, where *Bunte Trümmermassen* are already deposited with inverse stratigraphy. **c** Crystalline rock fragments and sediment-rock clasts settle and rotate (dashed arrow) on top of the *Bunte Trümmermassen* as irregular bodies and individual clasts before **d** turbulent (dashed arrow) suevite deposition

transported sediment-rock clasts (Oberbeck 1975; Hörz et al. 1983), which only experienced minor shock, were mixed with the shocked basement clasts. Suevite was subsequently deposited above the shocked basement clasts on top of the Bunte Breccia (Fig. 10d). The irregular distribution of basement clasts mixed with and overlying the sediment-rock-dominated apparently unshocked shocked components of the Bunte Breccia and directly overlain by suevite (Figs. 2,

3b-f), as well as the magnetic properties discussed by Sleptsova et al. (2024) are consistent to this emplacement mechanism, given the highly energetic and turbulent deposition of impact ejecta (Dressler and Sharpton 1997; Dressler and Reimold 2004; Kenkmann et al. 2014; Siegert et al. 2017).

The inverse stratigraphy as predicted by the Maxwell Z-model (Maxwell 1977; Croft 1980) is displayed in the Aumühle quarry from top to bottom as (i) crystalline

basement derived suevite (Figs. 2a, 3a–f), (ii) shocked basement clasts mixed with sediment-rock components (Figs. 2a, 3b–h), (iii) Bunte Breccia composed of upper Triassic sandstone (Fig. 3a), and (iv) Bunte Breccia consisting of upper Jurassic black shales (Fig. 3a).

## Conclusions

From our macroscopic observations and microfabric analysis of the moderately shocked basement clasts on top of the Bunte Breccia and directly overlain by suevite at the Aumühle quarry in the Ries impact structure, we conclude the following:

1. The different shock conditions of the moderately shocked basement clasts [shock stages up to F-S5 after Stöffler et al. 2018 (35–50 GPa) (Figs. 4, 5, 6, 7, 8)] and the intermixed apparently unshocked sediment-rock clasts (Fig. 9) reflect their different source localities within the impact structure (Fig. 10a).
2. The sharp boundaries between the impactite deposits (Figs. 2, 3) and missing impact-melt fragments associated with the basement clasts argue against their origin from the suevite upon turbulent deposition of the suevite on top of the Bunte Breccia. This is in agreement with the random orientation of the palaeomagnetic directions in the basement clasts as opposed to both the overlying suevites and the sediment-rock clasts in-between and at the bottom, which all show the palaeomagnetic field at the time of the impact (Sleptsova et al. 2024).
3. The metagranite cataclasite clast (Figs. 7, 8) indicates two stages of fracturing: one stage of in-situ cataclasis upon unloading from shock compression (Fig. 10a) and subsequent brecciation and transport of the basement clasts during crater excavation (Fig. 10b).
4. The shocked basement clasts were either injected within fractures of the transient crater wall or ballistically ejected on top of the somewhat earlier deposited components of the Bunte Trümmersmassen consistent with an inverse stratigraphy (Fig. 10c), where they were mixed with the sediment-rock clasts before emplacement of the suevite (Fig. 10d).

**Acknowledgements** The fieldwork and assistance with polarized light microscopy and SEM by Ayoub Benhoummad as well as assistance during sampling by Michael Wack are greatly acknowledged. We thank Jean Pohl for his helpful comments on the manuscript. We acknowledge the financial support of the Deutsche Forschungsgemeinschaft (TR534/9-1 and GI712/20-1).

**Funding** Open Access funding enabled and organized by Projekt DEAL.

**Data availability** Data will be made available upon request.

## Declarations

**Conflict of interest** No known competing financial interests or personal relationships influenced the results reported in this study.

**Open Access** This article is licensed under a Creative Commons Attribution 4.0 International License, which permits use, sharing, adaptation, distribution and reproduction in any medium or format, as long as you give appropriate credit to the original author(s) and the source, provide a link to the Creative Commons licence, and indicate if changes were made. The images or other third party material in this article are included in the article's Creative Commons licence, unless indicated otherwise in a credit line to the material. If material is not included in the article's Creative Commons licence and your intended use is not permitted by statutory regulation or exceeds the permitted use, you will need to obtain permission directly from the copyright holder. To view a copy of this licence, visit <http://creativecommons.org/licenses/by/4.0/>.

## References

- Abadian M (1972) Petrographie, Stoßwellenmetamorphose und Entstehung polymikter kristalliner Breccien im Nördlinger Ries. *Contrib Mineral Petrol* 35:245–262
- Abadian M, von Engelhardt W, Schneider W (1973) Spaltenfüllungen in allochthonen Schollen des Nördlinger Ries. *Geologica Bavarica* 67:229–237
- Arp G, Reimer A, Simon K, Sturm S, Wilk J, Kruppa C, Hecht L, Hansen BT, Pohl J, Reimold WU, Kenkmann T, Jung D (2019) The Erbisberg drilling 2011: Implications for the structure and postimpact evolution of the inner ring of the Ries impact crater. *Meteorit Planet Sci* 54:2448–2482. <https://doi.org/10.1111/maps.13293>
- Artemieva NA, Wünnemann K, Krien F, Reimold WU, Stöffler D (2013) Ries crater and suevite revisited-Observations and modeling Part II: Modeling. *Meteorit Planet Sci* 48:590–627. <https://doi.org/10.1111/maps.12085>
- Bader K, Schmidt-Kaler H (1977) Der Verlauf einer präriesischen Erosionsrinne im östlichen Riesvorland zwischen Treuchtlingen und Donauwörth. In: Schmidt-Kaler H (ed) *Geologica Bavarica* 75. Bayerisches Geologisches Landesamt, München, pp 401–410
- Bergerhoff G, Hundt R, Sievers R, Brown ID (1983) The inorganic crystal structure data base. *J Chem Inf Comput Sci* 23:66–69. <https://doi.org/10.1021/ci00038a003>
- Bischoff L, Oskierski W (1987) Fractures, Pseudotachylite Veins and Breccia Dikes in the Crater Floor of the Rochechouart Impact Structure, SW-France, as Indicators of Crater Forming Processes
- Borg IY (2013) Some Shock Effects in Granodiorite to 270 Kilobars at the Piledriver Site. In: Heard HC, Borg IY, Carter NL, Raleigh CB (eds) *Flow and Fracture of Rocks*. American Geophysical Union Geophysical Monograph Series, Washington DC, pp 293–311
- Bringemeier D (1994) Petrofabric examination of the main suevite of the Otting Quarry, Nordlinger Ries, Germany. *Meteoritics* 29:417–422. <https://doi.org/10.1111/j.1945-5100.1994.tb00607.x>
- Brückner LM, Trepmann CA (2021) Stresses during pseudotachylite formation - Evidence from deformed amphibole and quartz in fault rocks from the Silvretta basal thrust (Austria). *Tectonophysics* 817:229046. <https://doi.org/10.1016/j.tecto.2021.229046>
- Chao ECT (1967) Shock effects in certain rock-forming minerals. *Science* 156:192–202. <https://doi.org/10.1126/science.156.3772.192>
- Chao ECT (1976) Mineral-Produced High-Pressure Striae and Clay Polish: Key Evidence for Nonballistic Transport of Ejecta from

- Ries Crater. *Science* 194:615–618. <https://doi.org/10.1126/science.194.4265.615>
- Chao ECT, Hüttner R, Schmidt-Kaler H (1987) Aufschlüsse im Ries-Meteoriten-Krater. Bayerisches Geologisches Landesamt, München
- Croft SK (1980) Cratering flow fields: implications for the excavation and transient expansion stages of crater formation. *Geochim Cosmochim Acta Suppl* 14:2347–2378
- Davies GF (1972) Equations of state and phase equilibria of stishovite and a coesitelike phase from shock-wave and other data. *J Geophys Res* 77:4920–4933. <https://doi.org/10.1029/JB077i026p04920>
- Di Vincenzo G (2022) High precision multi-collector  $^{40}\text{Ar}/^{39}\text{Ar}$  dating of moldavites (Central European tektites) reconciles geochronological and paleomagnetic data. *Chem Geol* 608:121026. <https://doi.org/10.1016/j.chemgeo.2022.121026>
- Dressler BO, Reimold WU (2004) Order or chaos? Origin and mode of emplacement of breccias in floors of large impact structures. *Earth-Science Rev* 67:1–54. <https://doi.org/10.1016/j.earscirev.2004.01.007>
- Dressler BO, Sharpton VL (1997) Breccia formation at a complex impact crater: Slate Islands, Lake Superior, Ontario, Canada. *Tectonophysics* 275:285–311. [https://doi.org/10.1016/S0040-1951\(97\)00003-6](https://doi.org/10.1016/S0040-1951(97)00003-6)
- Fritz J, Greshake A, Stöffler D (2005) Micro-Raman spectroscopy of plagioclase and maskelynite in Martian meteorites: Evidence of progressive shock metamorphism. *Antarct Meteor Res* 18:96–116
- Graup G (1978) Das Kristallin im Nördlinger Ries - Petrographische Zusammensetzung und Auswurf mechanismus der kristallinen Trümmernmassen. Ferdinand Enke Verlag, Stuttgart, Struktur des kristallinen Untergrundes und Beziehungen zum Moldanubikum
- Graup G (1977) Die Petrographie der kristallinen Gesteine der Forschungsbohrung Nördlingen 1973. In: Schmidt-Kaler H (ed) *Geologica Bavarica* 75. Bayerisches Geologisches Landesamt, München, pp 219–229
- Holm-Alwmark S, Ferrière L, Alwmark C, Poelchau MH (2018) Estimating average shock pressures recorded by impactite samples based on universal stage investigations of planar deformation features in quartz—Sources of error and recommendations. *Meteorit Planet Sci* 53:110–130. <https://doi.org/10.1111/maps.13029>
- Hörz F (1965) Untersuchungen an Riesgläsern. *Beiträge Zur Mineral Und Petrogr* 11:621–661. <https://doi.org/10.1007/BF01128707>
- Hörz F, Ostertag R, Rainey DA (1983) Bunte Breccia of the Ries: continuous deposits of large impact craters. *Rev Geophys Sp Phys* 21:1667–1725
- Hörz F (1968) Statistical measurements of deformation structures and refractive indices in experimentally shock loaded quartz. In: French BM, Short NM (eds) *Shock metamorphism of natural materials*. Mono Book Corps, Baltimore, Maryland, pp 243–254
- Hüttner R, Schmidt-Kaler H (1999) Die Geologische Karte des Rieses 1: 50 000 (2., überarbeitete Auflage). *Geol Bavarica* 104:7–76
- Hüttner R (1969) Bunte Trümmernmassen und Suevit. In: Preuss E, Schmidt-Kaler H (eds) *Geologica Bavarica* 61. Bayerisches Geologisches Landesamt, Munich, pp 142–200
- Hüttner R (1977) Makroskopische Beobachtungen zur Deformation des Kristallins in der Forschungsbohrung Nördlingen 1973. In: Schmidt-Kaler H (ed) *Geologica Bavarica* 75. Bayerisches Geologisches Landesamt, pp 273–283
- Kenkmann T, Poelchau MH, Wulf G (2014) Structural geology of impact craters. *J Struct Geol* 62:156–182. <https://doi.org/10.1016/j.jsg.2014.01.015>
- Kieffer SW, Phakey PP, Christie JM (1976) Shock processes in porous quartzite: transmission electron microscope observations and theory. *Contrib Mineral Pet* 59:41–93. <https://doi.org/10.1007/BF00375110>
- Koch SA, Gilder SA, Pohl J, Trepmann C (2012) Geomagnetic field intensity recorded after impact in the Ries meteorite crater, Germany. *Geophys J Int* 189:383–390. <https://doi.org/10.1111/j.1365-246X.2012.05399.x>
- Kowitz A, Güldemeister N, Reimold WU, Schmitt RT, Wünnemann K (2013) Diaplectic quartz glass and SiO<sub>2</sub> melt experimentally generated at only 5 GPa shock pressure in porous sandstone: Laboratory observations and meso-scale numerical modeling. *Earth Planet Sci Lett* 384:17–26. <https://doi.org/10.1016/j.epsl.2013.09.021>
- Kowitz A, Güldemeister N, Schmitt RT, Reimold WU, Wünnemann K, Holzwarth A (2016) Revision and recalibration of existing shock classifications for quartzose rocks using low-shock pressure (2.5–20 GPa) recovery experiments and mesoscale numerical modeling. *Meteorit Planet Sci* 51:1741–1761. <https://doi.org/10.1111/maps.12712>
- Kring DA (2005) Hypervelocity collisions into continental crust composed of sediments and an underlying crystalline basement: Comparing the Ries (~24 km) and Chicxulub (~180 km) impact craters. *Chem Erde* 65:1–46. <https://doi.org/10.1016/j.chemer.2004.10.003>
- Kroepelin K, Wimmer K, Hoffmann VH (2022) Recent Observations in Suevite outcrops (Ries Impact, Germany). *Jahresberichte Und Mitteilungen Des Oberrheinischen Geol Vereins* 104:163–184. <https://doi.org/10.1127/jmoggv/104/0005>
- Lambert P (1981) Breccia dikes: geological constraints on the formation of complex craters. In: Schultz PH and Merrill RB (eds) *Multi-ring Basins*, Proc. Lunar Planet. Sci., 12A, p 59–78
- Lange J-M, Suhr P (2022) The distal Effects of the Ries Impact – a Synopsis. *Jahresberichte Und Mitteilungen Des Oberrheinischen Geol Vereins* 104:11–90. <https://doi.org/10.1127/jmoggv/104/0001>
- Leake BE, Woolley AR, Arps CES, Birch WD, Gilbert MC, Grice JD, Howthorne FC, Kato A, Kisch HJ, Krivovichev VG, Linthout K, Laird J, Mandarino JA, Maresch WV, Nickel EH, Rock NMS, Schumacher JC, Smith DC, Stephenson NCN, Ungaretti L, Whittaker EJW, Youzhi G (1997) Nomenclature of amphiboles: Report of the subcommittee on amphiboles of the international mineralogical association, commission on new minerals and mineral names. *Am Mineral* 82:1019–1037. <https://doi.org/10.1180/minmag.1997.061.405.13>
- Maxwell DE (1977) Simple Z model for cratering, ejection, and the overturned flap. In: Roddy DJ, Pepin RO, Merrill RB (eds) *Impact and Explosion Cratering*. Pergamon Press, New York, pp 1003–1008
- Mernagh TP (1991) Use of the laser Raman microprobe for discrimination amongst feldspar minerals. *J Raman Spectrosc* 22:453–457. <https://doi.org/10.1002/jrs.1250220806>
- Meyer C, Jébrak M, Stöffler D, Riller U (2011) Lateral transport of suevite inferred from 3D shape-fabric analysis: Evidence from the Ries impact crater, Germany. *Bull Geol Soc Am* 123:2312–2319. <https://doi.org/10.1130/B30393.1>
- Müller WF, Hornemann U (1969) Elektronenmikroskopischer Nachweis amorpher Bereiche in stoßwellenbeanspruchtem Quarz. *Naturwissenschaften* 56:279–279. <https://doi.org/10.1007/BF00633926>
- Newsom HE, Graup G, Iseri DA, Geissman JW, Keil K (1990) The formation of the Ries Crater, West Germany; Evidence of atmospheric interactions during a larger cratering event. In: Sharpton VL, Ward PD (eds) *Global catastrophes in Earth history; an interdisciplinary conference on impacts, volcanism, and mass mortality*: Geological Society of America Special Paper 247. pp 195–206
- Oberbeck VR (1975) The role of ballistic erosion and sedimentation in lunar stratigraphy. *Rev Geophys* 13:337–362. <https://doi.org/10.1029/RG013i002p00337>

- Osinski GR (2004) Impact melt rocks from the Ries structure, Germany: an origin as impact melt flows? *Earth Planet Sci Lett* 226:529–543. <https://doi.org/10.1016/j.epsl.2004.08.012>
- Osinski GR, Grieve RAF, Spray JG (2004) The nature of the groundmass of surficial suevite from the Ries impact structure, Germany, and constraints on its origin. *Meteorit Planet Sci* 39:1655–1683. <https://doi.org/10.1111/j.1945-5100.2004.tb00065.x>
- Osinski GR, Grieve RAF, Chanou A, Sapers HM (2016) The “suevite” conundrum, Part 1: The Ries suevite and Sudbury Onaping Formation compared. *Meteorit Planet Sci* 51:2316–2333. <https://doi.org/10.1111/maps.12728>
- Ostertag R (1983) Shock experiments on feldspar crystals. In: Proceedings of the 14th Lunar and Planetary Science Conference. pp B364–B376
- Pietrek A, Kenkmann T (2016) Ries Bunte Breccia revisited: Indications for the presence of water in Itzing and Otting drill cores and implications for the emplacement process. *Meteorit Planet Sci* 51:1203–1222. <https://doi.org/10.1111/maps.12656>
- Pohl J, Stöffler D, Gall H, Ernst K (1977) The Ries impact crater. In: Roddy DJ, Pepin RO, Merrill RB (eds) *Impact and Explosion Cratering*. Pergamon Press, New York, pp 343–404
- Reimold WU, McDonald I, Schmitt RT, Hansen B, Jacob J, Koeberl C (2013) Geochemical studies of the SUBO 18 (Enkingen) drill core and other impact breccias from the Ries crater, Germany. *Meteorit Planet Sci* 48:1531–1571. <https://doi.org/10.1111/maps.12175>
- Rocholl A, Böhme M, Gilg HA, Pohl J, Schaltegger U, Wijbrans J (2018) Comment on “A high-precision  $^{40}\text{Ar}/^{39}\text{Ar}$  age for the Nördlinger Ries impact crater, Germany, and implications for the accurate dating of terrestrial impact events” by Schmieder et al. (*Geochimica et Cosmochimica Acta* 220 (2018) 146–157). *Geochim Cosmochim Acta* 238:599–601. <https://doi.org/10.1016/j.gca.2018.05.018>
- Rooney TP, Riecker RE, Ross M (1970) Deformation twins in Hornblende. *Science* 169:173–175. <https://doi.org/10.1126/science.169.3941.173>
- Schaal RB, Hörz F (1977) Shock Metamorphism of Lunar and Terrestrial Basalts. *Proc Lunar Sci Conf* 2:1697–1729
- Schmidt-Kaler H (ed) (1977) *Ergebnisse der Ries-Forschungsbohrung 1973: Struktur des Kraters und Entwicklung des Kratersees*. Bayerischen Geologischen Landesamt, Munich
- Seybold L, Hölzl S, Trepmann C, Ernst V, Bahmer L (2022) Megablocks from the crystalline basement – the Lehberg outcrop, Unterwilflingen, Nördlinger Ries. *Jahresberichte Und Mitteilungen Des Oberrheinischen Geol Vereins* 104:147–161. <https://doi.org/10.1127/jmoghv/104/0004>
- Seybold L, Trepmann CA, Hölzl S, Pollok K, Langenhorst F, Dellefant F, Kaliwoda M (2023) Twinned calcite as an indicator of high differential stresses and low shock pressure conditions during impact cratering. *Meteorit Planet Sci* 19. <https://doi.org/10.1111/maps.14056>
- Siegert S, Branney MJ, Hecht L (2017) Density current origin of a melt-bearing impact ejecta blanket (Ries suevite, Germany). *Geology* 45:855–858. <https://doi.org/10.1130/G39198.1>
- Sleptsova IV, Gilder SA, Dellefant F, Trepmann CA, Ahanin N, Pohl J (2024) Thermal and Structural History of Impact Ejecta Deposits, Ries Impact Structure, Germany. *J Geophys Res Solid Earth* 129:1–23. <https://doi.org/10.1029/2023JB027460>
- Stähle V, Chanmuang NC, Schwarz WH, Trieloff M, Varychev A (2022) Newly detected shock-induced high-pressure phases formed in amphibolite clasts of the suevite breccia (Ries impact crater, Germany): Liebermannite, kokchetavite, and other ultrahigh-pressure phases. *Contrib to Mineral Petrol* 177:80. <https://doi.org/10.1007/s00410-022-01936-3>
- Stöffler D (1971a) Progressive metamorphism and classification of shocked and brecciated crystalline rocks at impact craters. *J Geophys Res* 76:5541–5551. <https://doi.org/10.1029/jb076i023p05541>
- Stöffler D (1971b) Coesite and stishovite in shocked crystalline rocks. *J Geophys Res* 76:5474–5488. <https://doi.org/10.1029/jb076i023p05474>
- Stöffler D (1972) Deformation and transformation of rock-forming minerals by natural and experimental shock processes. *Fortschritte Der Mineral* 49:50–113
- Stöffler D, Hornemann U (1972) Quartz and feldspar glasses produced by natural and experimental shock. *Meteoritics* 7:371–394
- Stöffler D, Langenhorst F (1994) Shock metamorphism of quartz in nature and experiment: I. Basic Observation and Theory *Meteoritics* 29:155–181. <https://doi.org/10.1111/j.1945-5100.1994.tb00670.x>
- Stöffler D, Ostertag R (1983) The Ries Impact Crater. *Fortschritte Der Mineral* 61:71–116
- Stöffler D, Artemieva NA, Wünnemann K, Reimold WU, Jacob J, Hansen BK, Summerson IAT (2013) Ries crater and suevite revisited—Observations and modeling Part I: Observations. *Meteorit Planet Sci* 48:515–589. <https://doi.org/10.1111/maps.12086>
- Stöffler D, Hamann C, Metzler K (2018) Shock metamorphism of planetary silicate rocks and sediments: Proposal for an updated classification system. *Meteorit Planet Sci* 53:5–49. <https://doi.org/10.1111/maps.12912>
- Stöffler D, Grieve RAF (2007) Impactites. In: Fettes D, Desmons J (eds) *Metamorphic Rocks: A Classification and Glossary of Terms, Recommendations of the International Union of Geological Sciences*. Cambridge University Press, Cambridge, pp 82–92, 111–125 and 126–242
- Stöffler D, Ewald U, Ostertag R, Reimold WU (1977) Research drilling Nördlingen 1973: Composition and texture of polymict impact breccias. In: Schmidt-Kaler H (ed) *Geologica Bavarica* 75. Bayerisches Geologisches Landesamt, Munich, pp 163–189
- Stöffler D (1977) Research drilling Nördlingen 1973: Polymict breccias, crater basement, and cratering model of the Ries impact structure. In: Schmidt-Kaler H (ed) *Geologica Bavarica* 75. Bayerisches Geologisches Landesamt, Munich, pp 163–189
- Sturkell EFF, Ormö J (1997) Impact-related clastic injections in the marine Ordovician Lockne impact structure, Central Sweden. *Sedimentology* 44:793–804. <https://doi.org/10.1046/j.1365-3091.1997.d01-54.x>
- Sturm S, Wulf G, Jung D, Kenkmann T (2013) The Ries impact, a double-layer rampart crater on earth. *Geology* 41:531–534. <https://doi.org/10.1130/G33934.1>
- Sturm S, Kenkmann T, Willmes M, Pösges G, Hiesinger H (2015) The distribution of megablocks in the Ries crater, Germany: Remote sensing, field investigation, and statistical analyses. *Meteorit Planet Sci* 50:141–171. <https://doi.org/10.1111/maps.12408>
- Tartèse R, Endley S, Joy KH (2022) U-Pb dating of zircon and monazite from the uplifted Variscan crystalline basement of the Ries impact crater. *Meteorit Planet Sci* 57:830–849. <https://doi.org/10.1111/maps.13798>
- von Engelhardt W (1990) Distribution, petrography and shock metamorphism of the ejecta of the Ries crater in Germany—a review. *Tectonophysics* 171:259–273. [https://doi.org/10.1016/0040-1951\(90\)90104-G](https://doi.org/10.1016/0040-1951(90)90104-G)
- von Engelhardt W (1997) Suevite breccia of the Ries impact crater, Germany: Petrography, chemistry and shock metamorphism of crystalline rock clasts. *Meteorit Planet Sci* 32:545–554. <https://doi.org/10.1111/j.1945-5100.1997.tb01299.x>
- von Engelhardt W, Graup G (1984) Suevite of the Ries crater, Germany: Source rocks and implications for cratering mechanics. *Geol Rundschau* 73:447–481. <https://doi.org/10.1007/BF01824968>
- von Engelhardt W, Arndt J, Fecker B, Pankau HG (1995) Suevite breccia from the Ries crater, Germany: Origin, cooling history and devitrification of impact glasses. *Meteoritics* 30:279–293. <https://doi.org/10.1111/j.1945-5100.1995.tb01126.x>
- Wones DR, Eugster HP (1965) Stability of biotite: Experiment, theory, and application. *Am Mineral* 50:1228–1272

Wright Horton J, Gibson RL, Reimold WU, Wittmann A, Gohn G, Edwards L (2009) Geologic columns for the ICDP-USGS Eyreville B core, Chesapeake Bay impact structure: Impactites and crystalline rocks, 1766 to 1096 m depth. *Spec Pap Geol Soc Am* 458:21–49. [https://doi.org/10.1130/2009.2458\(02\)](https://doi.org/10.1130/2009.2458(02))

Wünnemann K, Morgan JV, Jödicke H (2005) Is ries crater typical for its size? An analysis based upon old and new geophysical data and

numerical modeling. In: Kenkmann T, Hörz F, Deutsch A (eds) *Large meteorite impacts III: Geological Society of America Special Paper 384*. Geological Society of America, Boulder, pp 67–83